mater.scichina.com link.springer.com

Published online 13 May 2024 | https://doi.org/10.1007/s40843-023-2884-8
Sci China Mater 2024, 67(6): 1684–1705

SPECIAL TOPIC: Advanced Energy Catalytic Materials

Copper-based catalysts for carbon monoxide electroreduction to multi-carbon products

Wen Zhao[1], Juan Liu[1], Guangtao Wang[1], Xintian Wang[1], Chuanju Yang[1], Jian Li[2], Yuting Wang[1], Xiaolian Sun[3], Richen Lin[4], Gancheng Zuo[1,5] and Wenlei Zhu[1*]

ABSTRACT **Electrochemical carbon dioxide reduction (ECO_2R) is an attractive pathway to store carbon and renewable energy as chemical bonds in multi-carbon products. However, the complex multi-step reaction processes set huge obstacles for the direct conversion of CO_2 to C_{2+} products. A strategy that uses carbon monoxide (CO) as a "transfer station" to produce C_{2+} at improved selectivity and reaction rates *via* the tandem ECO_2R to CO and electrochemical CO reduction (ECOR) has attracted a lot attention. In this review, we focus on the design strategy of Cu-based electrocatalysts toward the formation of specific C_{2+} products in ECOR. Representative design strategies for catalysts engineering are summarized in various aspects, and the most recent research in the improvement of electrolysis reactor is included. Finally, the main challenges and the future prospects in this research field are expounded. These insights and perspectives offer meaningful guidance for designing Cu-based electrocatalytic system with enhanced C_{2+} product selectivity.**

Keywords: CO electroreduction, Cu-based catalysts, multi-carbon products

INTRODUCTION

To alleviate the greenhouse effect and energy crisis [1–13], electrochemical CO_2 reduction (ECO_2R) is a carbon-neutral route for the transformation of CO_2 into marketable multi-carbon hydrocarbons and oxygenates (C_{2+}) using renewable energy [4,14–24]. However, the direct reduction of CO_2 to C_{2+} products is significantly affected by severe carbonation in alkaline conditions and hydrogen evolution in acidic conditions, both of which impact reaction activity and selectivity [25–31]. It is well established that the CO_2-to-CO conversion has achieved remarkable selectivity close to 100% [32–38]. The conversion of CO to C_{2+} products can be achieved through Fischer-Tropsch (F-T) synthesis [39–41], which currently still suffers from high reaction temperatures (230–450°C) and huge demand for hydrogen [42–44]. Recently, a cascade reduction approach, where CO_2 is reduced to CO in the first step followed by CO electroreduction, results in much higher C_{2+} selectivity and carbon efficiency [32,45–47]. Furthermore, the electrochemical CO reduction (ECOR) technique is usually conducted in a water-based electrolyte at ambient temperature, with water acting as the proton source [48–51]. For a long time, ECOR has followed the research paradigm established by ECO_2R. Therefore, using ECOR as a downstream technique of ECO_2R presents a promising approach for the resource utilization of CO_2 (Fig. 1).

To accomplish selective and efficient ECOR, electrocatalysts are required to reduce the reaction energy barrier in the formation of C_{2+} products and improve the kinetics of the C–C coupling process [52,53]. Thence, mechanism-oriented design of catalysts becomes paramount in order to augment the CO-to-C_{2+} performance. So far, considerable research efforts have been devoted to developing catalytic materials in ECOR [54,55]. Among various kinds of electrocatalysts, copper (Cu)-based catalysts, which exhibit suitable binding energy for *CO and *H, facilitate C–C coupling and thus generate C_{2+} products [56]. Typical methods of catalyst engineering, such as doping and alloying [57–59], morphology control [60], surface modification [61,62], *in-situ* reconstruction [63,64], and defect engineering [65], have been applied to improve the performance of ECOR on the Cu-based catalysts. Moreover, since ECOR is sensitive to the reaction environment, it is also crucial to mediate the transport and coverage of reacting species by designing the electrodes and catalyst supports, which can influence the reaction pathway [66–68].

Thus far, only a handful of review papers on ECOR have been published, which primarily provide an overview of Cu-based designs from a product formation perspective, rather than

[1] State Key Laboratory of Pollution Control and Resource Reuse, Frontiers Science Center for Critical Earth Material Cycling, State Key Laboratory of Pollution Control and Resource Reuse, the Frontiers Science Center for Critical Earth Material Cycling, School of the Environment, Nanjing University, Nanjing 210023, China
[2] State Key Laboratory of Analytical Chemistry for Life Science, School of Chemistry and Chemical Engineering, Nanjing University, Nanjing 210023, China
[3] State Key Laboratory of Natural Medicines, Key Laboratory of Drug Quality Control and Pharmacovigilance, School of Pharmaceutics, China Pharmaceutical University, Nanjing 210009, China
[4] Key Laboratory of Energy Thermal Conversion and Control of Ministry of Education, School of Energy and Environment, Southeast University, Nanjing 211189, China
[5] Jiangsu Engineering Lab of Water and Soil Eco-remediation, School of Environment, Nanjing Normal University, Nanjing 210023, China
* Corresponding author (email: wenleizhu@nju.edu.cn)

 © Science China Press 2024

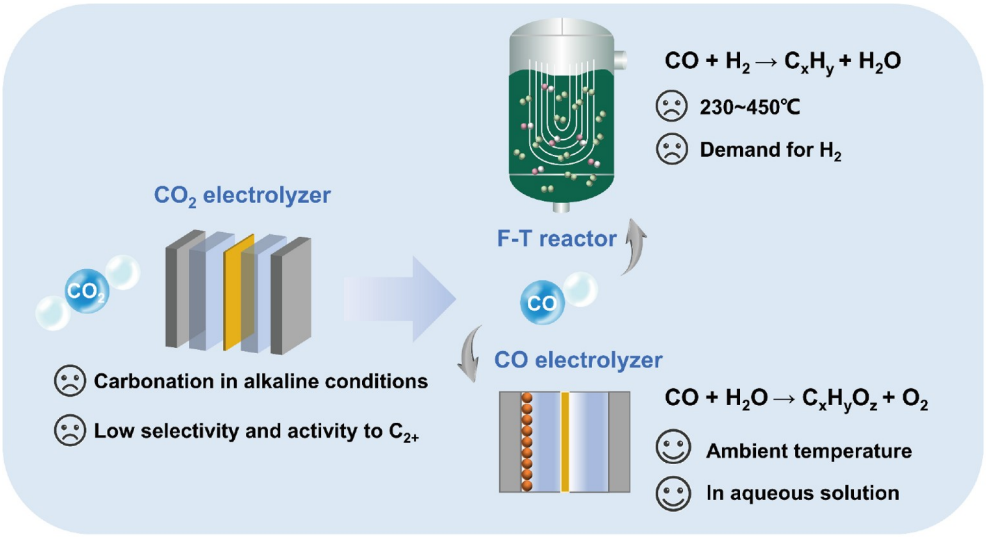

Figure 1 Schematic illustration of the cascade reduction and the comparison of F-T synthesis and ECOR.

emphasizing the clear and effective design strategies of Cu-based catalysts [45,69]. This review zooms in on the recent development of highly efficient Cu-based catalysts in the ECOR process. Firstly, the fundamental aspects will be discussed from the performance evaluation factors to the formation mechanisms of various C_{2+} products. Next, the most representative upgrade strategies for Cu-based catalysts in terms of catalyst engineering and system design will be summarized. Finally, based on the main challenges and the future prospects in this research direction, this review offers meaningful guidance for performance optimization of ECOR through the rational design of Cu-based catalysts.

PERFORMANCE EVALUATION FOR ECOR

For lab-scale evaluation of ECOR technologies, the selectivity for a single product, the activity and the stability of overall system are typically reported as performance indicators. All of the ECOR standard potentials here are calculated *via* the Gibbs free energy of reaction [4]. A typical commercial catalyst would require a Faradaic efficiency of more than 90% with a stability of thousands of hours, which is cost-competitive with fossil fuel-derived sources [70]. The overpotential should be less than 0.4 V *vs*. reversible hydrogen electrode (RHE) with a current density of higher than 200 mA cm^{-2} [71,72]. To date, considerable research has led to progress in selectivity, activity, and stability. Even so, there is still a lack of excellent work to integrate these advantages. The quest for commercialization continues to be a great impetus to optimize the catalytic transformations, and the current state of ECOR to target products is presented in Table 1.

Selectivity

For complex reactions that produce different products, the aim is to maximize yield and purity of the target product. The selectivity of ECOR is usually assessed based on the Faraday efficiency (FE) of the reduction products, which reflects the proportion of electrons transferred to the desired product. The FE for products is calculated using the following equation:

$$FE = z \times n \times F / Q,$$

where z, n, F and Q are the electron transfer number (Table 1), the mole fraction of the product, the Faraday's constant and the total charge during the reaction, respectively. The high selectivity conversion of carbon monoxide can effectively reduce the subsequent product separation costs.

Activity

The electrocatalytic activity is the degree to which an electrocatalyst accelerates a reaction, which can be evaluated by the overpotential value at a specified current density, or the current density at a specified overpotential. The current density is usually defined as the electrical current flow per geometric area of the electrode. High current density means high formation rate of the target product, which is desirable for lowering capital costs. From industrial consideration, industrially relevant current densities of several hundreds of mA cm^{-2} (>200mA cm^{-2}) are required to be applied with catalyst loadings as high as 1–2 mg cm^{-2} [76,77]. The overpotential can be termed additional potential to drive a certain reaction due to kinetic activations, limited mass transport and ohmic resistances between the anode and the cathode [72]. A low overpotential reduces the total electrical energy input and minimizes the electricity cost.

Stability

Stability usually refers to the duration for which the catalyst performance is maintained at a certain level of activity and selectivity. Notably, under commercially relevant current densities of >200 mA cm^{-2}, catalysts often undergo particle agglomeration, active-phase change, and/or element dissolution, making the long-term operational stability a considerable challenge [78,79]. In the current ECOR research, most of the stability tests are completed in the membrane electrode assembly (MEA), where results show significant improvement over those obtained from the H-cell and the flow cell. However, the evaluation of stability is subject to laboratory test conditions, and the current test duration is typically less than 100 h. This is far below the level required for achieving a large-scale electrocatalytic process [80].

MECHANISMS INVESTIGATION

The conversions of CO to C_{2+} products, including ethanol,

© Science China Press 2024

ethylene, acetate, and propanol, all involve various reaction pathways that include a carbon–carbon (C–C) coupling step. However, it is still controversial how the C_1 intermediates (such as *CO, *COH and *CHO) perform C–C coupling reactions (Fig. 2). After the initial activation of CO on the active surface to form *CO (where * denotes a binding site), the intermediate proceeds through the hydrogenation reaction to give *CHO or *COH, representing as a C-pathway or an O-pathway [73], respectively. Xiang *et al.* [81] proposed that the C-pathway to yield the *CHO intermediate is thermodynamics-controlled, while the O-pathway to produce the *COH intermediate is kinetics-controlled. In addition, the dimerization of *CO species was also proposed to form the C–C bond. Montoya *et al.* [82] calculated the barriers of C–C coupling on Cu(111) and (100) and found them to be sufficiently low for CO dimerization to proceed before CO reduction. Generally, there is consensus that the C–C coupling reaction is structure-sensitive, pH-dependent, and potential-dependent, which aligns with the ongoing debates in the vast body of theoretical research and experimental results [83–85].

Ethanol and ethylene

It has been suggested that there is a shared pathway for the formation of ethanol and ethylene, both of which are formed through a certain oxygen-containing intermediate [86,87]. *CO–COH is known to be a common intermediate proposed in the literature to give C_{2+} products [88,89]. Koper's group [90] proposed that *CO–CHO is less stable than *CO–COH by 0.16 eV, suggesting a more favorable initial hydrogenation of the O atoms in $*C_2O_2$. Deriving from *CO–COH, *CHCOH is suggested to participate in the formation of ethanol and ethylene. The hydrogenation and the dihydroxylation of *CHCOH form CHCHOH* and CCH*, respectively (Fig. 3a) [73]. Density functional theory (DFT) calculations in terms of the adsorption energy of key intermediates in Fig. 3b show that CCH* formation is thermodynamically more favorable than CHCHOH* formation by 0.32 eV on Cu(100), which therefore results in the higher selectivity towards C_2H_4 than EtOH. On Cu(111), the two competitive steps have equivalent ΔG, suggesting similar selectivity towards C_2H_4 and CH_3CH_2OH. However, on Cu(110), CHCHOH* is preferred over CCH* for formation (by 0.17 eV), indicating a higher selectivity towards EtOH [91]. Besides, Lum *et al.* [92] proposed that oxygen in the product might arise from water rather than from CO. As shown in Fig. 3c, *(^{16}OH)C–CH contributes to either (^{16}O)ethanol or (^{18}O)ethanol formation.

Acetate

Recently, acetate has emerged as a prominent product in ECOR, particularly in the multi-component system [93]. Starting from CO, acetate is produced through the ethenone intermediate (Fig. 4a) [94]. Koper and Calle-Vallejo [90] first proposed the possibility of the *C=C=O intermediate, postulating it as an

Table 1 ECOR half-reactions for C_{2+} products and the current state of electrocatalytic performance

Possible ECOR half-reactions toward C_{2+}	Electrode potentials (*vs.* RHE)	FE (%)	Current density (mA cm^{-2})	Stability (h)	Ref.
$2CO\ (g) + 8H^+ + 8e^- \rightarrow C_2H_4\ (g) + 2H_2O\ (l)$	0.28	72	>800	2	[73]
$2CO\ (g) + 8H^+ + 8e^- \rightarrow C_2H_5OH\ (l) + H_2O\ (l)$	0.30	68.8	111	100	[74]
$2CO\ (g) + 4H^+ + 4e^- \rightarrow CH_3COO^-\ (l)$	0.34	91 ± 2	112	820	[57]
$3CO\ (g) + 12H^+ + 12e^- \rightarrow C_3H_7OH\ (l) + 2H_2O\ (l)$	0.43	47 ± 3	38	110	[75]

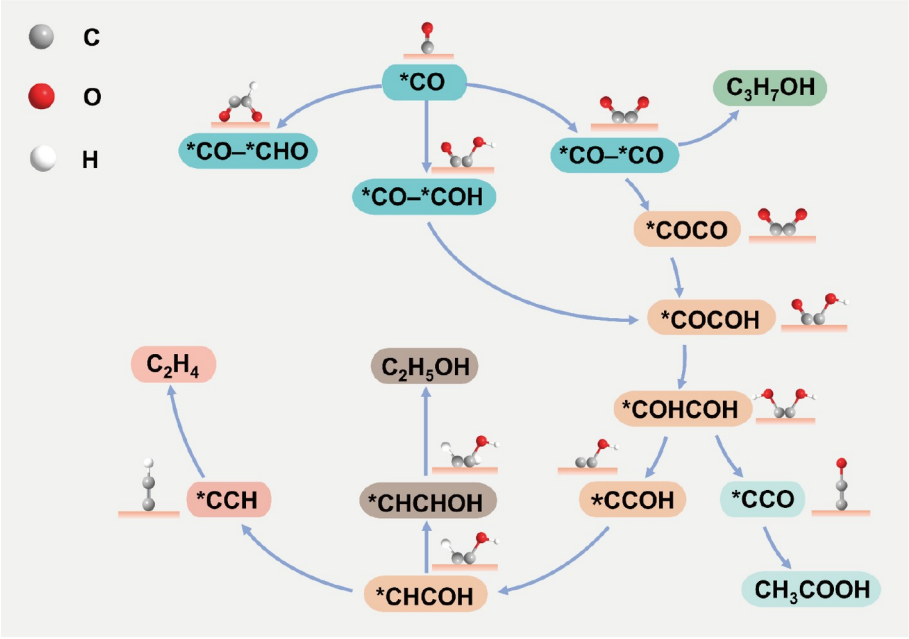

Figure 2 Possible reaction pathways for the formation of C_{2+} products based on the key intermediates.

© Science China Press 2024

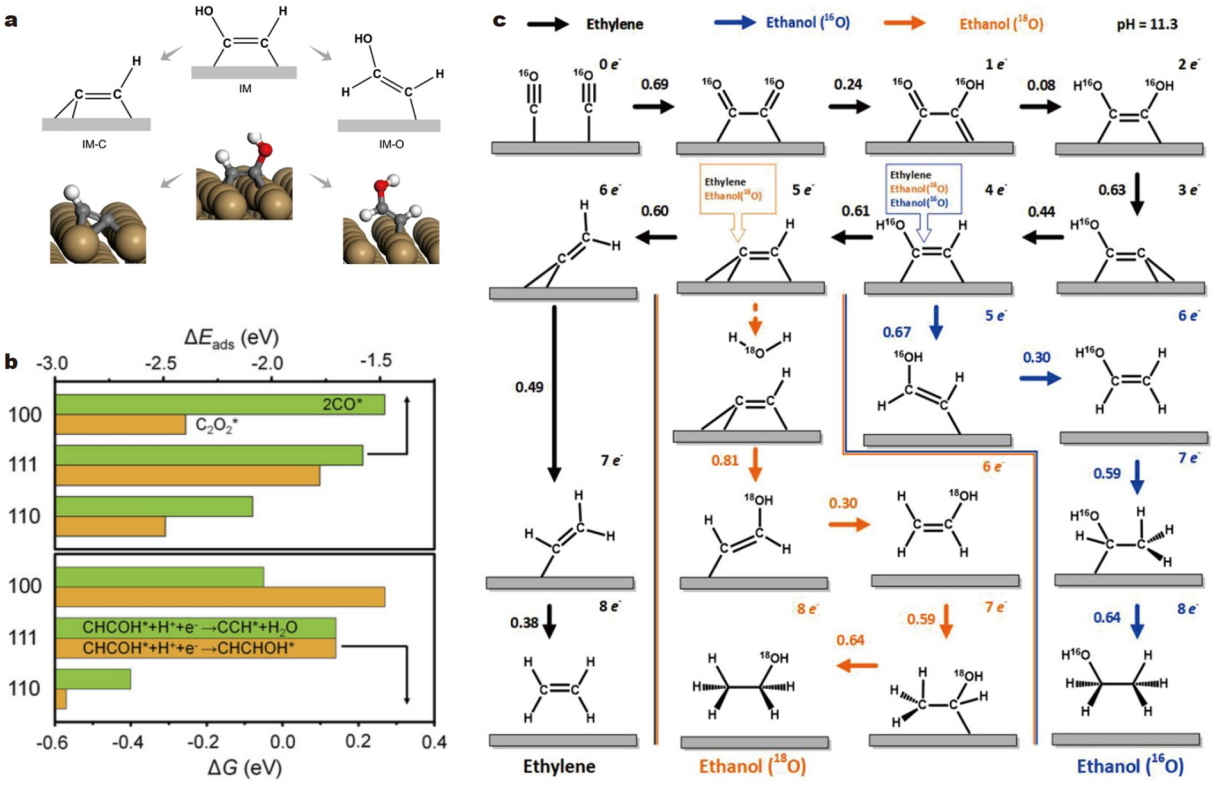

Figure 3 (a) Schematic plot of the reaction mechanism where the last oxygen-containing group in *CHCOH (IM) is removed, forming *CCH (IM-C), and an alternative pathway to *CHCHOH (IM-O), as well as the geometries of IM, IM-C and IM-O on Cu(100) surfaces. Yellow, copper; grey, carbon; red, oxygen; white, hydrogen. Reprinted with permission from Ref. [73], Copyright 2019, Springer Nature. (b) The adsorption energies of key intermediates that affect activity (upper panel) and free energies of competitive pathways for C_2H_4 and EtOH formation (lower panel) on Cu(100), Cu(111), and Cu(110). Reprinted with permission from Ref. [91], Copyright 2020, Wiley-VCH Verlag GmbH & Co. KGaA, Weinheim. (c) Mechanistic pathways for CO reduction predicted from full-solvent quantum mechanics (QM)-based molecular metadynamics to obtain free energy reaction barriers at 298 K. Reprinted with permission from Ref. [92], Copyright 2018, American Chemical Society.

intermediate in the ethylene pathway. However, later extensive works proposed that *(OH)C=COH → *C=C=O possesses a one-to-one mapping to acetate [57,95].

Jiao's group [95] proposed that *C=C=O prefers high pH and less negative potential. As shown in Fig. 4b, the proposed pathways assumed that acetate forms through direct reaction of OH^- with *C=C=O to form *C=C(OH)O$^-$ (ΔG = 0.72 eV), in agreement with the experimental observation that highly alkaline environments favor the formation of acetate [95,96]. Moreover, Wei *et al.* [97] proposed that the switch in selectivity from ethylene to acetate is primarily driven by the coverage of absorbed CO (*CO) (Fig. 4c). According to the DFT calculation results, CO preferentially adsorbs on terrace sites at low CO pressure and inclines to generate ethylene, whereas step sites are provided with more CO at high CO pressure, and thus, acetate production is substantially improved.

Propanol

The underlying mechanism of propanol production *via* ECOR is complex. It is generally accepted that the reduction of CO to C_3 products first requires a C_1–C_1 coupling step, followed by a C_1–C_2 coupling step [98,99]. Therefore, it is essential to prevent the individual conversion of C_1 and C_2 intermediates directly into final products. The confinement effect has been applied to boost C_3 production *via* the nanocavity strategy [100,101]. According to DFT calculations, CO is abundant on the surface due to its strong adsorption energy compared that that of CO_2. Consequently, the coupling of C_2 and CO is assumed to be one of the most likely pathways for C_3 formation (Fig. 5a). In subsequent research, Pang *et al.* [98] proposed that the interface between Cu (111) and Cu(100) lowers the barriers of both the CO–CO and CO–OCCO coupling steps compared with the individual facets (Fig. 5b). More recently, the successive proton coupled electron transfer (PCET) reactions from the CCO* species were investigated by Fontecave and coworkers [59]. The formed CHCO*, CHCHO*, CH2CHO*, and CH_3CHO* intermediates can undergo a coupling reaction with CO* to form different C_3 surface intermediates and produce propanol in subsequent steps (Fig. 5c).

In summary, a range of intermediates is primarily produced through hydrogenation or dihydroxylation of specific key intermediates. The reaction barrier varies depending on different conditions, including factors of catalysts engineering (such as exposed facets) or system design (such as pH and CO coverage), resulting in distinct pathways stemming from a shared intermediate. Further discussion on these two aspects provides insight into the formation mechanism of propanol and other multi-carbon products, thus offering effective guidance for the development of high-performance ECOR catalysts.

Cu-BASED CATALYSTS ENGINEERING

In this section, we will introduce several strategies aimed at

© Science China Press 2024

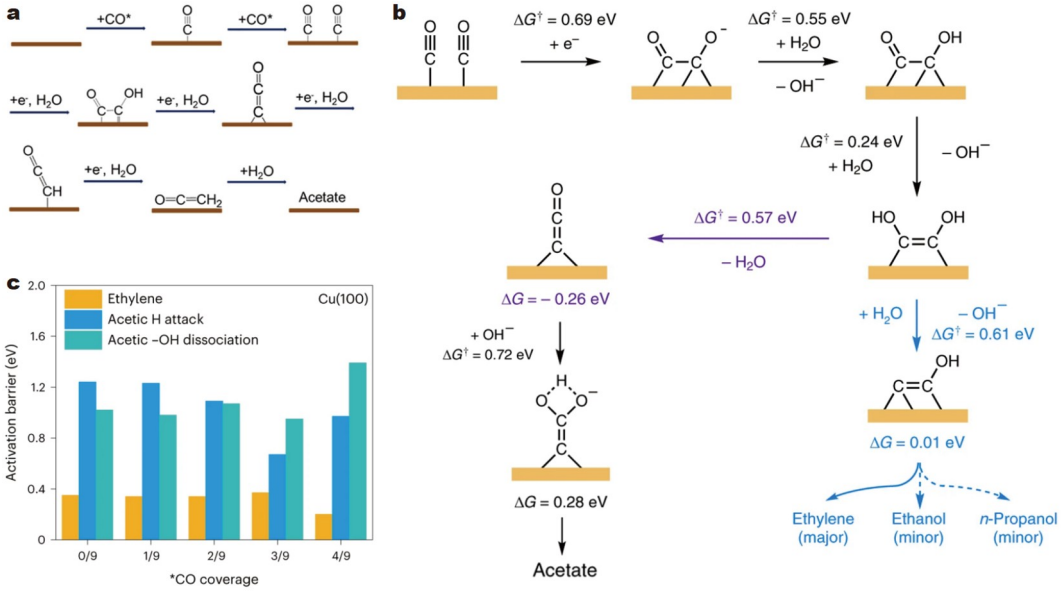

Figure 4 (a) Proposed mechanism for the electroreduction of CO to acetate. Reprinted with permission from Ref. [94], Copyright 2023, American Chemical Society. (b) Mechanism for CO-to-acetate *via* OH^- attack. Reprinted with permission from Ref. [95], Copyright 2019, Springer Nature. (c) Activation free-energy barriers of ethylene as well as acetate *via* H attack and –OH dissociation on Cu(100). Reprinted with permission from Ref. [97], Copyright 2023, Springer Nature.

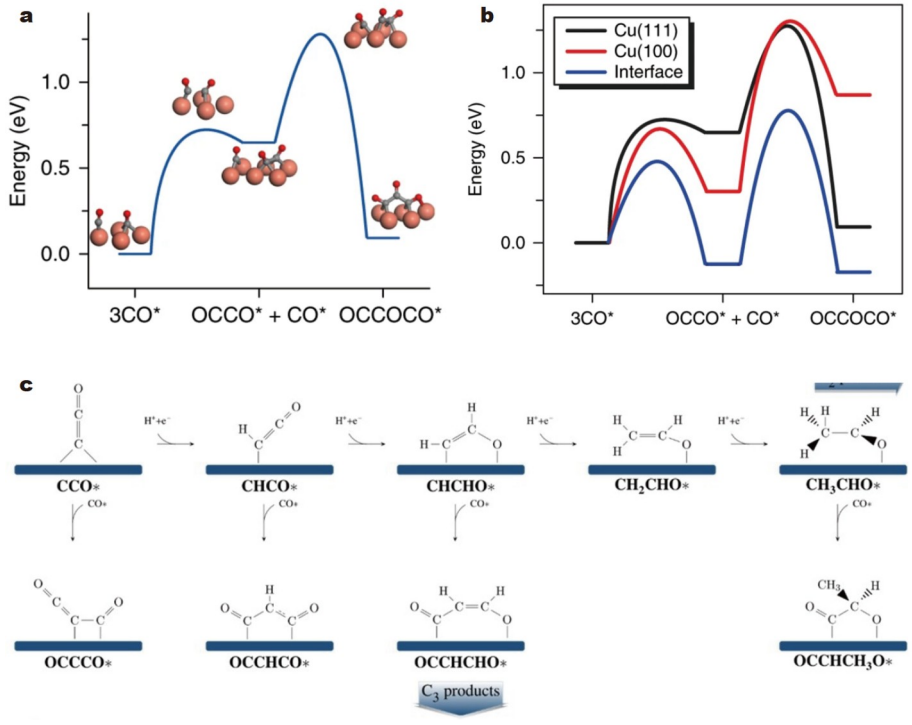

Figure 5 (a) Energy profile of the C_3 formation intermediates. The geometries of intermediate states and transition states are shown as insets (only the CO species in the reaction are illustrated). Red, oxygen; grey, carbon; orange, copper. Reprinted with permission from Ref. [100], Copyright 2018, Springer Nature. (b) The energy profiles of CO–CO and CO–OCCO dimerizations on Cu(111), Cu(100) and the interface. Reprinted with permission from Ref. [98], Copyright 2019, Springer Nature. (c) Selected elementary steps of the mechanism for the reduction of CO to C_3 products. Reprinted with permission from Ref. [59], Copyright 2023, Wiley-VCH GmbH.

improving the performance of Cu-based catalysts in ECOR, including doping and alloying, morphology control, surface modification, *in situ* reconstruction and defect engineering.

Doping and alloying

For heterogeneous metal catalysts, compositions are engineered *via* doping or alloying to maximize the catalytic performance [102–105]. Doping involves introducing a trace of impurities into a pure metallic sample, while maintaining the crystalline structure of the metal [106]. Alloying does modify this structure forming chemical bonds between the host and guest metals [107]. But when the dopants tend to be metal elements, doping

 © Science China Press 2024

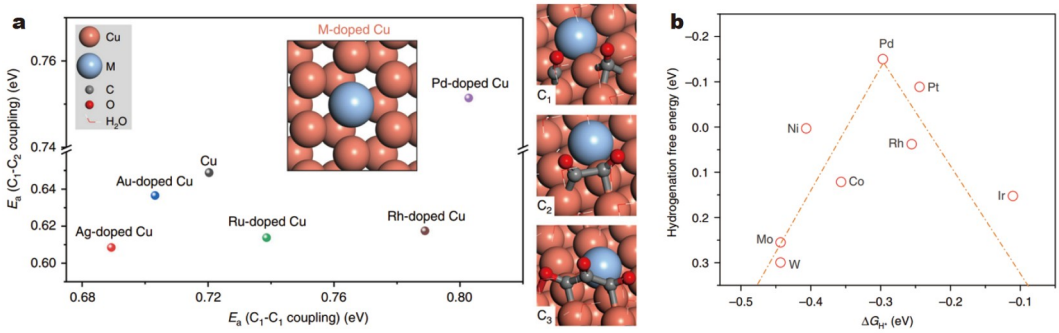

Figure 6 (a) DFT calculated reaction barriers (E_a) for C_1–C_1 and C_1–C_2 couplings on screened M-doped Cu systems. Reprinted with permission from Ref. [110], Copyright 2019, The Author(s). (b) Plot of the calculated hydrogenation reaction free energies of HOCCH* against the H adsorption energies of different dopants. Reprinted with permission from Ref. [111], Copyright 2020, The Author(s).

and alloying strategy are frequently used in modifying the electronic properties of catalysts without highlighting the difference.

Since foreign atoms are incorporated into the host material, the interaction between the valence orbital of the transition metal and the electron orbital of the adsorbate will cause surface strain, thus affecting the adsorption energy for the catalyst to the key intermediates [108,109]. At present, several M-doped Cu systems (M = Ag, Au, Ru, and Pd) have attracted much attention in ECOR. Sargent's group [110] carried out DFT calculations to reveal the barrier of C–C coupling of different bimetallic catalysts (Fig. 6a). They found that Ag-doped Cu possesses the lowest activation energies for C–C coupling. Although Pd-doped Cu exhibits relatively high activation energies, Pd, when used as a dopant, exhibits appropriate hydrogenation reaction free energies of HOCCH* and H-absorption abilities, as shown in other work (Fig. 6b) [111]. In addition, as shown in Fig. 6a, Au and Ru are suitable dopants for C_1–C_1 coupling and C_1–C_2 coupling, respectively.

The introduction of Ag mainly affects the C–C coupling step and the adsorption configuration of reaction intermediates. Sargent's group [112] reported that the Ag-Cu_2O catalysts synthesized *via* a kinetically restricted galvanic replacement between Cu_2O and Ag^+ ions (Fig. 7a) reached an acetate FE of 70% and a full-cell energy efficiency of 25% at the optimal Ag:Cu loading (Fig. 7b). The presence of new active sites promoted the surface CO dimerization by suppressing the competing HER reaction, and the preferential destabilization of intermediates along the ethylene and ethanol pathway promoted acetate selectivity through the *CCO intermediate, as supported by the DFT study. Similarly, Lu's group [113] proposed that the Ag-modified, oxide-derived (OD) Cu catalysts, prepared *via* high-energy ball milling, exhibited near 80% FEs for C_{2+} liquid products (Fig. 7d). The optimal selectivity for C_{2+} liquid products was achieved with atomic ratio of Cu:Ag of 0.8:0.2. Representative surface-enhanced infrared absorption (SEIRA) spectra of Cu(OD) and $Cu(OD)_{0.8}Ag_{0.2}$ are shown in Fig. 7c. This substantial difference suggests that the introduction of Ag in the sample decreases the average binding strength of CO likely by introducing weak binding sites that are distinct from sites on the Cu surface. More recently, Pang's group [57] examined a series of Cu-in-N dilute alloys (DAs; N = Ag, Au, Pd, Pt, Ni) for the reaction energies of *(HO)C=COH → *C=C=O and *(HO)C=COH → *C=COH. It was found that the use of Ag as Cu hosts favors monodentate-binding *C=C=O over bidentate-binding *C=COH, thus promoting the selective formation of acetate (Fig. 7e). They achieved a CO-to-acetate FE of 91% with CO gas at 10 atm (1 atm = 1.01×10^5 Pa, Fig. 7f), as well as an FE of 85% with an 820-h operating time (Fig. 7g), which were the highest known selectivity and stability for acetic acid to date.

When Pd as a dopant is introduced to Cu-M system, it is very likely that the hydrogenation step can significantly affect the reaction pathway [114]. Li *et al.* [111] proposed that incorporating Pd in Cu can moderate hydrogen adsorption and assist the hydrogenation of C_2 intermediates, thereby providing an approach to favor alcohol production and suppress ethylene. Given the composition-dependent electrocatalytic performance, the $CuPd_{0.007}$ catalyst delivered a peak $FE_{alcohol}$ of 40%, at −0.62 V *vs.* RHE (Fig. 8a). According to extended X-ray absorption fine structure (EXAFS) spectra of different CuPd catalysts, a pure Pd-Cu contribution from $CuPd_{0.007}$ was observed; whereas, an additional Pd–Pd bond formation was observed for the $CuPd_{0.011}$ (Fig. 8b). The results indicated that an optimal loading of Pd on Cu may be the decisive factor for achieving a desirable reaction, because the aggregation of Pd leads to excessive H adsorption, thus promoting the formation of H_2 rather than C_{2+} products. It also confirms the role of atomic-level doping in steering post C–C coupling reactions toward C_{2+} products. In subsequent research, Shen *et al.* [115] reported Cu-Pd bimetallic electrocatalysts exhibiting high selectivity toward acetate. They proposed the reaction pathway with *CO–*CHO following a CO hydrogenation step, in agreement with the argument of Pd-induced lower hydrogenation free energy (Fig. 8c). Moreover, the $Cu_{49}Pd_{51}$ catalyst produced acetate dominantly throughout the investigated potential range (Fig. 8d). The composition dependence can be attributed to the excess Pd aggregation in the Pd-rich catalyst. Zheng's group [116] proposed an atomically ordered copper-palladium intermetallic compound (Fig. 8e) to enhance the adsorption and coverage of surface *CO, and achieve a 500-h CO-to-acetate conversion at 500 mA cm^{-2} with a stable acetate FE of ~50%. The ordered Cu-Pd sites can avoid excessive binding with carbonic species, thereby maximizing the effect of adsorption enhancements. This is in agreement with the report that Pd binds carbon-based species more strongly than Cu [117]. According to the DFT calculation, the *H binding energy on CuPd(110) was lower than that on Pd(111). This decreased *H adsorption was attributed to the occupation of hollow sites consisting of Cu and Pd atoms by *CO, which sank *H below the surface and thus inhibited H_2 evolution.

In addition to Ag and Pd, Au and Ru are also used as dopants

© Science China Press 2024

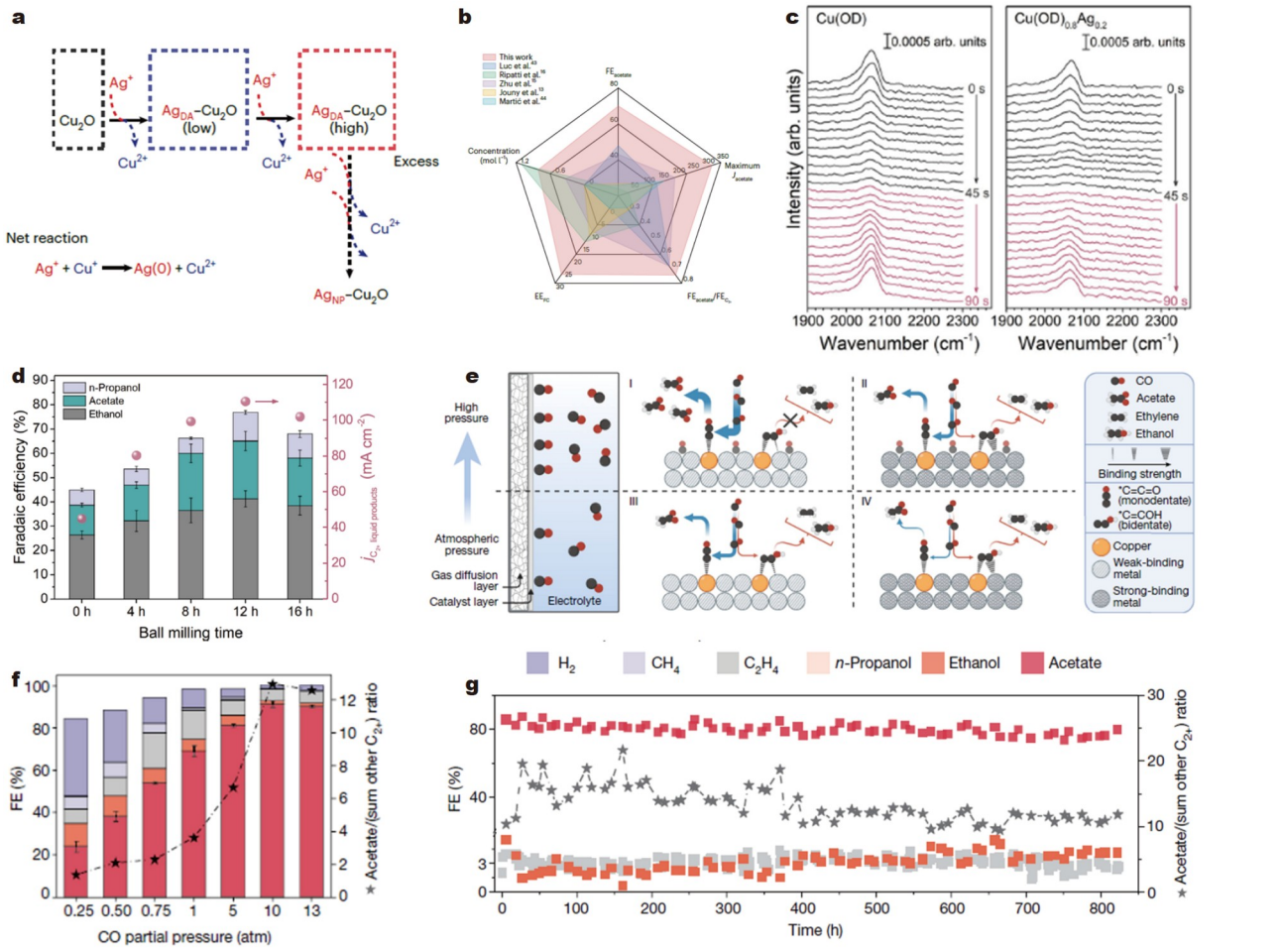

Figure 7 (a) Synthetic scheme for the AgCu DA bimetallic catalyst materials through a galvanic replacement reaction. (b) Comparison of the performance metrics of Ref. [112] and other relevant references. Reprinted with permission from Ref. [112], Copyright 2023, Springer Nature. (c) Representative time evolution of the infrared bands that result from CO bound to the Cu surface recorded after removing CO in bulk solution by pulsing Ar-saturated electrolyte and subsequently delivering CO-saturated electrolyte at 45 s. (d) Ball milling time-dependent FE of multi-carbon liquid products. Reprinted with permission from Ref. [113], Copyright 2023, The Author(s). (e) Schematic illustration of design matrix considering both CO pressure and host metal for Cu/M-DA materials. (f) Effect of CO partial pressure with a potential of −0.57 V *vs.* RHE in 5 M KOH. (g) Demonstration of stable operation: Cu/Ag-DA in a 10-atm MEA cell during 820 h of electrolysis at 100 mA cm^{-2} current density in 2.5 M KOH. Reprinted with permission from Ref. [57], Copyright 2023, Springer Nature.

to improve C_{2+} activity and selectivity. Zhao's group [94] fabricated Cu-Au alloys with atomically isolated Au atoms on the Cu host by a one-step reduction (Fig. 9a). Gold is an effective electrocatalyst to enhance the *CO coverage on Cu and accelerate C–C bond formation [118]. As a result, 1% Au-doped Cu(111) exhibited superior activity of the reduction of CO to acetate on the microporous layer (MPL) with 2 mg cm^{-2} carbon black (Fig. 9b). Sargent's group [119] prepared a Ag-Ru-Cu catalyst (Fig. 9c, d) *via* a two-step galvanic replacement. In contrast to Ag-Cu catalyst system, the introduction of Ru further increases the average *CO adsorption energy and thus results in higher *CO coverage on the surface. As a result, a high *n*-propanol (*n*-PrOH) FE of 36% ± 3% was achieved using a Ag-Ru-Cu catalyst (Fig. 9e).

Morphology control

The morphology of electrocatalysts can play a role in their catalytic performance for ECOR [120,121]. One the one hand, catalysts with various morphologies expose specific facets to enhance activity and selectivity of specific products [122,123]. One the other hand, the confinement effect produced by the cavity structure leads to the local enrichment of intermediates to promote C–C coupling reactions in a confinement space [124,125]. To date, it has been found that Cu-based nanowires, nanosheets, nanoparticles (NPs), and nanocavities show different product distributions in the performance of CO-to-C_{2+} electroreduction.

Cu-based nanowires were synthesized to investigate the relationships between the surface structures and the catalytic performance, on the basis of which DFT calculations were conducted to elucidate possible reaction pathways on different facets of Cu nanowires. Wang's group [126] reported that the coordinately unsaturated (110) surface sites on the Cu nanowires were responsible for the selective reduction of CO to C_{2+} species at low overpotential. In terms of the free energy of CO-to-C_{2+} *via* CHO–CHO or C–C coupling mechanism, Cu(110) is more thermodynamically favored than (211), (100), and (111). Kang's group [127] reported a two-dimensional triangular-shaped Cu

 © Science China Press 2024

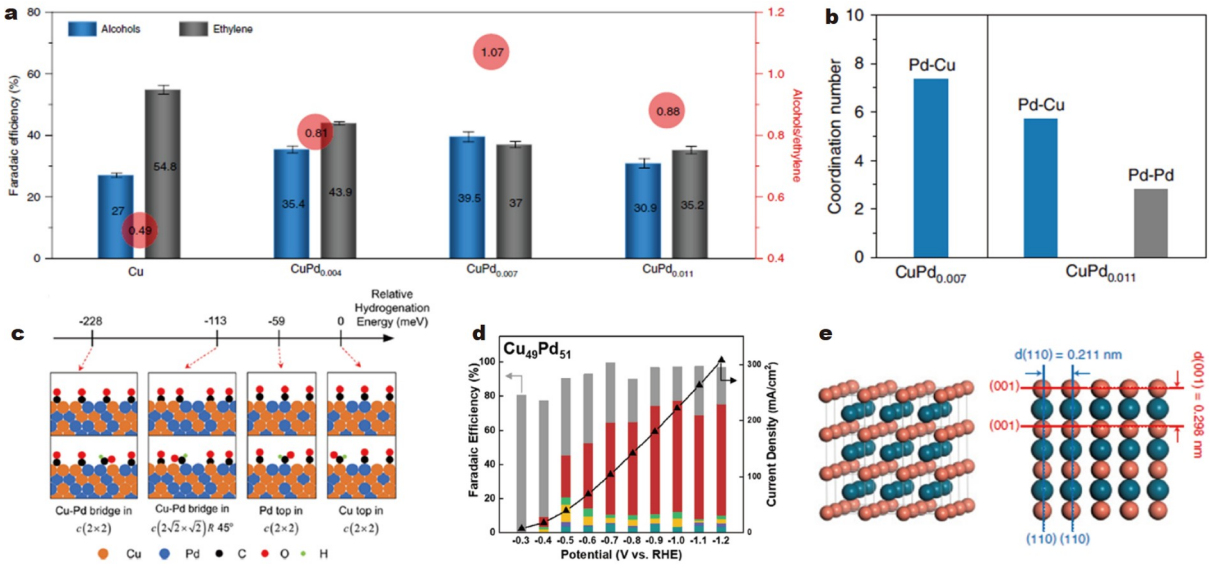

Figure 8 (a) Productions on Cu, $CuPd_{0.004}$, $CuPd_{0.007}$ and $CuPd_{0.011}$ catalysts at various applied potentials (*vs.* RHE) in 1 M KOH. (b) Simulated coordination numbers of $CuPd_{0.007}$ (left) and $CuPd_{0.011}$ (right). Reprinted with permission from Ref. [111], Copyright 2020, The Author(s). (c) Relative hydrogenation energies for *CO on the various catalyst surfaces. (d) FEs and geometric current densities measured for the electroreduction of CO on $Cu_{49}Pd_{51}$. Reprinted with permission from Ref. [115], Copyright 2022, American Chemical Society. (e) Crystal structure of CuPd with ordered, body-centred cubic structure and its projection in the [1 − 10] direction. Reprinted with permission from Ref. [116], Copyright 2022, Springer Nature.

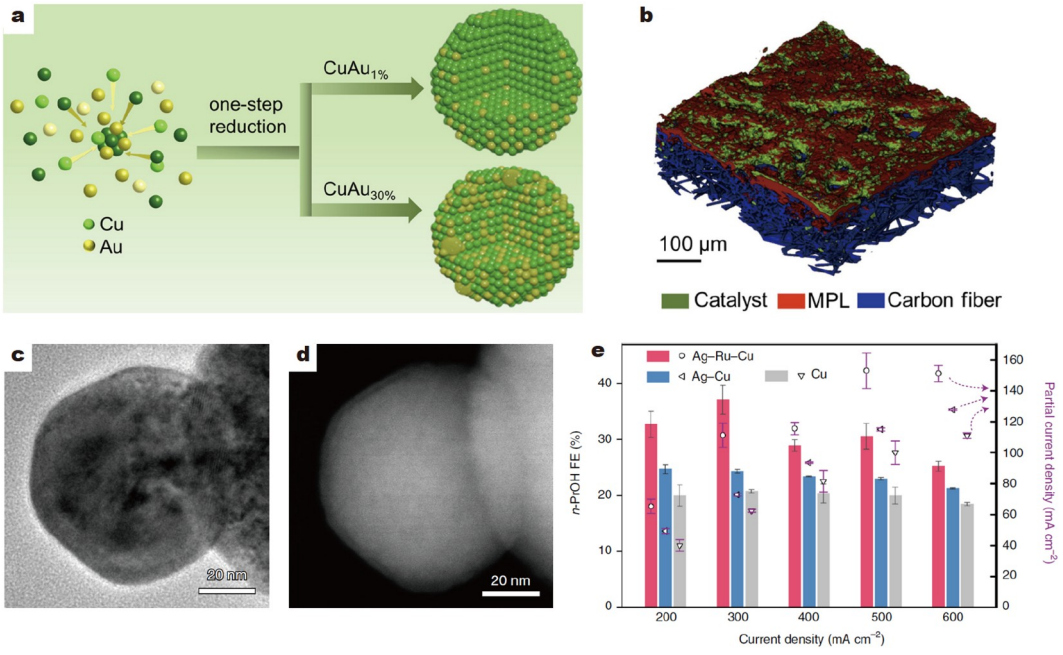

Figure 9 (a) Schematic illustration of $CuAu_{1\%}$ and $CuAu_{30\%}$ preparation. (b) X-ray computed tomography of $CuAu_{1\%}$ on homemade gas diffusion layers with 2 mg cm^{-2} carbon black. Reprinted with permission from Ref. [94], Copyright 2023, American Chemical Society. (c) Bright-field scanning transmission electron microscopy (STEM) image and (d) high-angle annular dark-field STEM (HAADF-STEM) image of the Ag-Ru-Cu catalyst. (e) *n*-PrOH FEs and partial *n*-propanol current densities on different electrodes at various current densities. Reprinted with permission from Ref. [119], Copyright 2022, Springer Nature.

nanosheet, which selectively exposed Cu (111) facets (Fig. 10a, b). The extraordinarily stable (111) surface enhanced acetate formation while suppressing ethylene and ethanol formation (Fig. 10c). Sargent's group [98] reported NPs consisting of highly fragmented copper structures with a mixture of Cu (111) and Cu(100) facets (Fig. 10d–f). Since the Cu(111) facet is C_1 selective and the Cu(100) facet is C_2 selective, additional opportunities for C_1 and C_2 intermediates to become coupled are created. As a representative work, Zhao's group [60] proposed a morphology-controlled synthesis strategy without any capping agents (surfactants, polymers, small adsorbates, or biomolecules) to present the intrinsic catalytic performance of catalysts. They synthesized a series of Cu_2O nanocrystals by combining the concentration depletion effect and the oxidation etching process

© Science China Press 2024

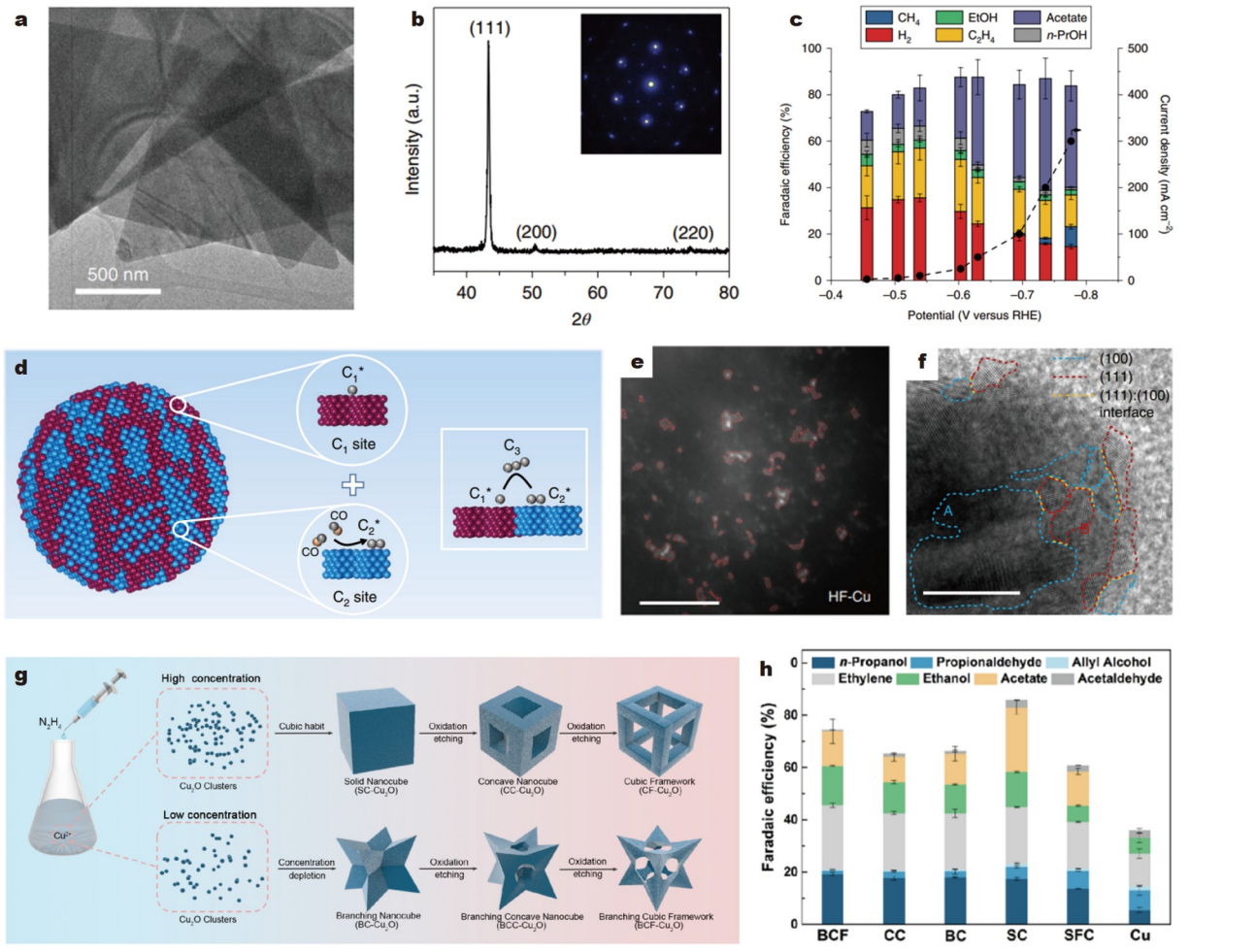

Figure 10 (a) TEM image of triangular Cu nanosheets. (b) XRD pattern of Cu nanosheets assembled on a Si wafer, which preferentially shows the (111) peak. Inset: selected area electron diffraction (SAED) pattern of Cu nanosheets. (c) Total current densities and cumulative FEs *vs.* applied potentials for CO electroreduction on Cu nanosheets in 2 M KOH. Reprinted with permission from Ref. [127], Copyright 2019, Springer Nature. (d) The catalyst with highly mixed nanofragments of the Cu(200) and Cu(111) facets may bring the optimal C_1 and C_2 sites into physical proximity, contributing with one another to the coupling of C_1–C_2 and then the coupling into C_3 products. (e) The dark-field-TEM image highlights the Cu(111) and Cu(100) facets of catalysts HF-Cu. Scale bar: 100 nm. (f) The high-resolution TEM image shows facet information for the catalysts HF-Cu. Scale bar: 10 nm. Reprinted with permission from Ref. [98], Copyright 2019, Springer Nature. (g) Illustration of concentration depletion and oxidation etching effects between different morphologies of Cu_2O nanocrystals. (h) FEs of C_{2+} products of COR for the catalysts derived from surfactant-free Cu_2O nanocrystals at −0.45 V *vs.* RHE. Reprinted with permission from Ref. [60], Copyright 2022, American Chemical Society.

(Fig. 10g), and enhancing the electrocatalytic performance for the conversion of CO to *n*-propanol. They found the Cu_2O branching cubic framework derived catalyst (BCF-Cu_2O) presents the highest *n*-propanol current density among the series (Fig. 10h), which may be attributed to its exposed facets. According to DFT calculations, it is easier to form OCCO* intermediates on the (100) facet and the exposure of the (110) facet would facilitate the coupling of the OCCO* dimer with a third CO*. Therefore, the coexistence of clean Cu(100) and Cu (110) is more conducive to the formation of C_3 products.

Catalysts with a confinement space appear to be more efficient in promoting the generation of C_3 products. Zhuang *et al.* [100] reported that Cu_2O NPs were synthesized into three-dimensional nanocavity Cu catalysts by an *in situ* electroreduction strategy, and the results showed that the higher C_3 production had a correlation with the morphology-driven confinement effect (Fig. 11a, b). According to the finite-element method (FEM) simulations, they found that the cavity restricts the outflow of locally produced C_2 species, which leads to higher local C_2 intermediate concentration inside the cavity, and ultimately generates a heightened C_3 production rate inside the cavity (Fig. 11c, d). More recently, Du *et al.* [128] conducted an investigation of the multi-shell structured Cu catalysts (Fig. 11e). They demonstrated that the enrichment of C_1 and C_2 intermediates by nanoconfinement space led to the possibility of further coupling. Notably, the Raman peaks (Fig. 11f) of Cu-CO stretching over the $Cu_2O@)_2Cu_2O$ catalyst were stronger in comparison to those with other catalysts under the same conditions, which indicated that the catalyst with a multi-shell structure possessed a stronger Cu-CO adsorption ability, thus contributing to the subsequent C_1–C_1 and C_1–C_2 coupling (Fig. 11g).

Surface modification

The adhered organic molecules with different electronic properties can influence the local environment of catalyst surface by

 © Science China Press 2024

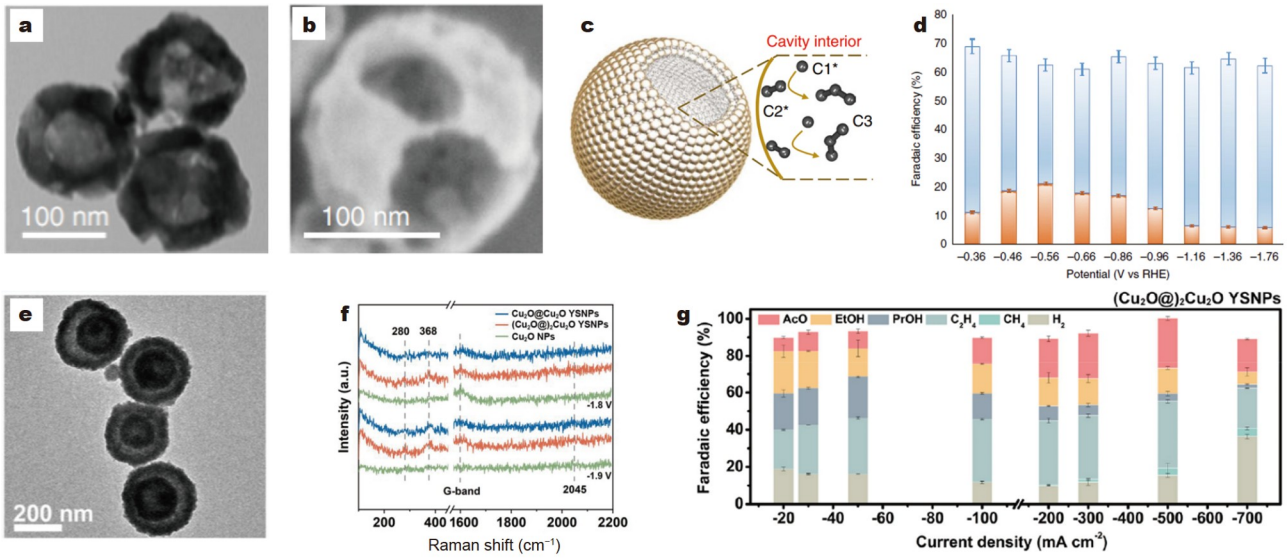

Figure 11 (a) TEM and (b) scanning electron microscopy (SEM) images for the cavity structure. (c) The schematic shows how the cavity confinement effect promotes C_2 species binding and further conversion to C_3. *: the surface species. (d) FEs of C_2 products (acetate, ethanol and ethylene) (blue) and C_3 propanol (orange) on the nanocavity Cu catalysts under a range of applied potentials. Reprinted with permission from Ref. [100], Copyright 2018, Springer Nature. (e) TEM images of Cu_2O@Cu_2O yolk–shell nanoparticles (YSNPs). (f) *Operando* Raman spectroscopy of Cu_2O NPs/GDE, Cu_2O@Cu_2O YSNPs/GDE, and $(Cu_2O@)_2Cu_2O$ YSNPs/GDE under CO conditions. (g) ECOR product distribution of $(Cu_2O@)_2Cu_2O$ YSNPs at each given current density in 1.0 M KOH under ambient conditions. Reprinted with permission from Ref. [128], Copyright 2023, American Chemical Society.

tuning interactions among reactants and intermediates, thereby favoring the stabilization of key intermediates for more selective ECOR to C_{2+} products [129,130]. Ji and coworkers [131] reported a copper NP/polypyrrole (Cu-Ppy) nanowire, which was fabricated by the assembly of metallic Cu NPs with Ppy nanowires (Fig. 12a, b). The Cu-Ppy composite catalyst enabled selective CO electroreduction toward C_2H_4, with an FE of 69% at −0.78 V *vs.* RHE. As the Ppy coating stabilizes OCCO*, a key intermediate to produce C_2H_4, both the activity and selectivity of Cu-Ppy for CO-to-C_2H_4 were enhanced (Fig. 12c). Moreover, a coordination polymer (CP) catalyst containing Cu(I)-imidazole coordination bonds for CO-to-acetate conversion was reported by Luo and coworkers (Fig. 12d) [62]. From DFT calculations, the catalytic sites of the CP structure are the isolated Cu site, where the enthalpy changes of HOCCOH* to OCC* are more negative than that of HOCCOH* to HOCC*, suggesting the high selectivity toward acetate. As a result, the CP catalyst enabled a 61% FE toward acetate at a current density of 400 mA cm^{-2} (Fig. 12e). In subsequent research, Wang *et al.* [132] reported an amino functionalized Cu surface (Cu@NH_2) and elucidated the effect of the amino groups on the Cu surface based on a combination of *in situ* spectroscopy studies and DFT calculations (Fig. 12f, g). The authors found that the presence of surface amino groups could stabilize the *CHO intermediate through hydrogen bonding, thereby increasing the coverage of *CHO on the catalyst's surface to facilitate the process of *CO–*CHO coupling to acetate with an FE of 51.5% and an acetate partial current density of around 150 mA cm^{-2} (Fig. 12h).

In-situ reconstruction

By designing metal oxides and complexes precursors, which will undergo substantial atomistic reconstruction under reducing conditions, the electrocatalyst properties can be affected [133–136]. Generally, the reconstruction strategy for Cu-based compounds leads to a significant structure evolution during the ECOR process. The *in situ* generated interface, the oxygen species and ligands on the catalyst surface will create new active centers to decrease the energy barrier of the C–C coupling reaction for C_{2+} products [137,138].

OD-Cu has been proven as a group of efficient electrocatalysts for ECO_2R, which derives from reconstructed Cu oxide such as CuO and Cu_2O (Cu_xO) [139]. The *in situ* generated Cu_xO/Cu interface plays a key role in ECOR, rather than the initial copper oxide [140,141]. OD-Cu catalysts have been shown to yield a high selectivity toward oxygenates *vs.* hydrocarbons [142,143]. Pioneer development of OD-Cu in ECOR was demonstrated by Kanan and coworkers [144]. The nanocrystalline Cu prepared from Cu_2O produced C_{2+} products with 57% FE, which outperformed Cu NPs. Higher surface roughness factor and density of grain boundaries (GBs) are attributed to the enhanced CO reduction activity and selectivity [145,146]. Long *et al.* [147] presented a directed reconstruction strategy by introducing Au NPs to steer the formation of abundant undercoordinated Cu sites. In the presence of Au NPs, the Cu atoms tend to rearrange into a disordered surface, bearing more disordered Cu atoms around Au NPs (Fig. 13a). Furthermore, it is highly desirable to investigate stable Cu compounds as alternatives to Cu_xO as starting materials for electrochemical *in situ* reconstruction and its effect on ECOR performance. For example, Schmid and coworkers [148] reported 92% FE for CO reduction to C_{2+} at 600 mA cm^{-2} using $Ag_2Cu_2O_3$ as a catalyst template to *in situ* form CuAg bimetallic material. The surface valence band X-ray photoelectron spectroscopy (XPS) spectra of the mentioned materials are shown in Fig. 13b, where the position of the d-band center is shifted significantly away from a monometallic Cu surface. By analyzing the mass spectrometry data in Fig. 13c, they proposed that the available electrons were exclusively used to drive the reduction of $Ag_2Cu_2O_3$ in the first 75 s.

Besides, copper-based catalysts derived from metal-organic complexes also demonstrated good performance for ECOR. Du

© Science China Press 2024

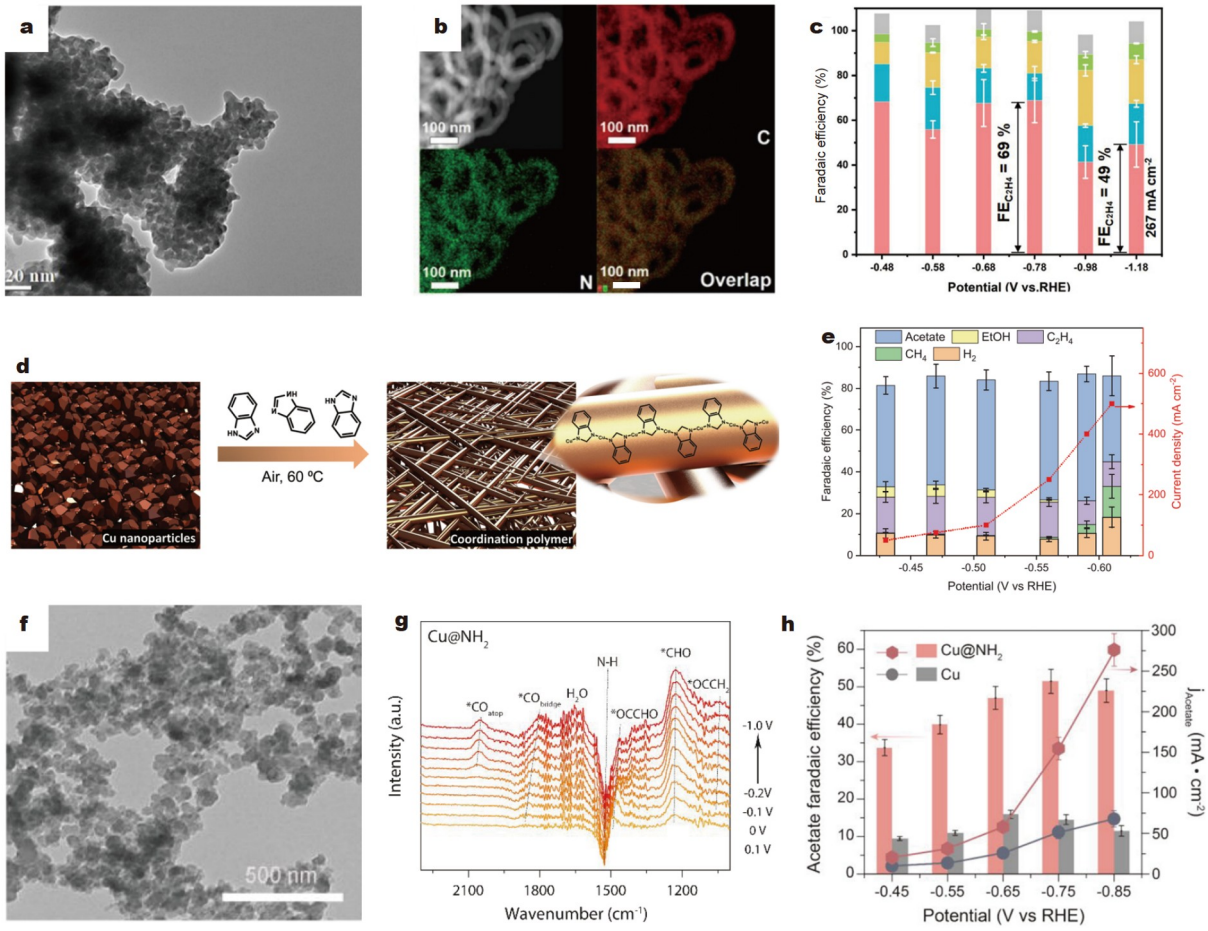

Figure 12 (a) TEM image of Cu NPs. (b) Energy-dispersive X-ray spectroscopy elemental mappings of Ppy NWs. (c) FE values for all products *vs.* applied potentials of Cu-Ppy composite. Reprinted with permission from Ref. [131], Copyright 2021, Elsevier. (d) Schematic of the synthesis process for CP catalyst. (e) Current density and FE as a function of the applied potential for ECOR on CP catalyst in 3 M KOH. Reprinted with permission from Ref. [62] , Copyright 2022, Wiley-VCH Verlag GmbH. (f) TEM image of Cu@NH_2. (g) *In situ* attenuated total reflection surface enhanced infrared absorption spectroscopy (ATR-SEIRAS) recorded during CO electroreduction on Cu@NH_2. (h) Acetate FE and partial current density *vs.* the applied potential for CO electroreduction on Cu@NH_2 in CO-saturated 1.0 M KOH solution. Reprinted with permission from Ref. [132], Copyright 2023, American Chemical Society.

et al. [63] employed cuprous 7,7,8,8-tetracyanoquinodimethane (CuTCNQ) as the precursor to form N-containing Cu NPs (N-Cu NPs) catalyst. They found the occurrence of structure evolution and the existence of residual organic ligands in the reconstructed catalysts under reductive conditions according to the Fourier transform infrared (FTIR) spectrum (Fig. 13d). The XPS spectra in the Cu 2p and C 1s regions for N-Cu NPs and CuTCNQ show the changes in the local electronic environment during the CO reduction process. More electrons are transferred from C atoms to N atoms as the enhanced C–N binding energy is observed in the C 1s regions. Then, as expected, the electron cloud densities of Cu atoms increased due to the connection with N atoms. Thus, the formed N-Cu NPs acted as the active center and it can be anticipated that the reconstructed N-Cu NPs with unique structural features would present enhanced ECOR performance. Impressively, the electrocatalyst presented the highest FE of 81.31% towards multi-carbon products at −0.69 V *vs.* RHE (Fig. 13e). Similarly, Rong *et al.* [149] reported a strategy for highly selective production of acetate from CO electrolysis by constructing metal-organic interfaces, which were constructed by *in situ* reconstruction of Cu complexes. The reconstructed copper phthalocyanine (CuPc) catalyst achieves a high FE of 84.2% for acetate production and an acetate partial current density as high as 605 mA cm^{-2} (Fig. 13f). The time-dependent X-ray diffraction (XRD) shows the gradual disappearance of characteristic peaks of the crystal structure of β-phase CuPc (Fig. 13g). In addition, they prepared a control electrode with the absence of organic ligands (CuPc-after-wash), possessing a similar Cu loading to the CuPc electrode. Consequently, that Raman peak is invisible over the CuPc-after-wash electrode, while a very broad Raman peak appears at 1800–2100 cm^{-1} assigned to the adsorption of *CO in CuPc electrode, pointing out the vital role of newly-formed metal-organic interfaces in facilitating *CO adsorption on Cu.

Defect engineering

Structural defects have been extensively used to tune the catalytic activity [150–152]. So far, point defects and planar defects have been introduced to Cu-based catalysts for ECOR. The defects can change the surface properties thus optimizing the binding energy or adsorption energy of reaction intermediates, regulating the reaction pathway [153]. In addition, defects can change the reaction environment and increase the number of active sites to promote the reduction reaction [154]. In this section, several kinds of defects, including vacancy, GBs and stacking faults (SFs), are presented.

© Science China Press 2024

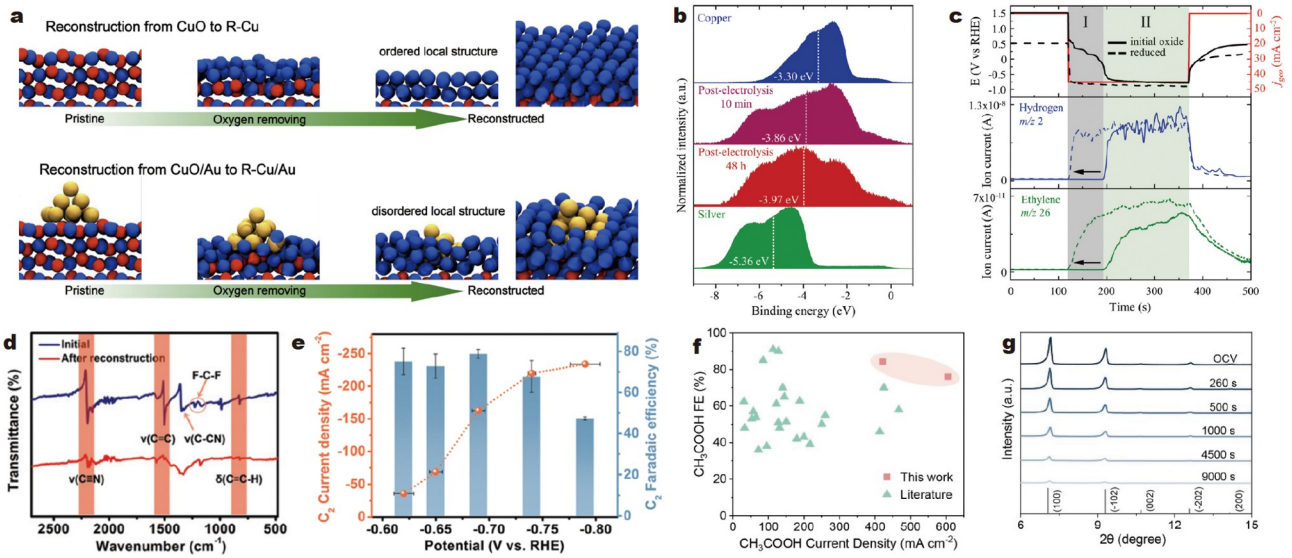

Figure 13 (a) Snapshots of the simulated reconstruction processes from CuO to R-Cu and CuO/Au to R-Cu/Au. Reprinted with permission from Ref. [147], Copyright 2024, American Chemical Society. (b) *Ex situ* surface valence band XPS spectra belonging to reference copper and silver foils, and the fully reduced post-electrolysis catalyst samples which were characterized after being exposed to reaction conditions for 10 min and 48 h. (c) The applied current density (45 mA cm^{-2}), measured potentials at the cathode and resulting signals for ethylene and hydrogen are shown *vs.* time. Reprinted with permission from Ref. [148], Copyright 2020, Royal Society of Chemistry. (d) FTIR spectra of CuTCNQ/GDL and N-Cu NPs/GDL. (e) C_2 FE and the corresponding partial current density of N-Cu NPs/GDL at each given potential in 1.0 M KOH. Reprinted with permission from Ref. [63], Copyright 2022, Royal Society of Chemistry. (f) Performance comparison for CO electrolysis to acetate. (g) Time-dependent XRD patterns of the CuPc electrode after CO electrolysis at 500 mA cm^{-2}. Reprinted with permission from Ref. [149], Copyright 2023, Wiley-VCH Verlag GmbH.

Vacancy is a point defect where atoms are missing at lattice junction positions. Oxygen vacancy (Ov) is the most common anion vacancy exhibiting low formation energy and significantly affects the surface electronic structure [155,156]. Huang's group [157] sprayed Cu atoms onto CeO_2 nanorods and found that Cu atoms at the interface coordinate with Ce atoms due to the formation of Ov (Fig. 14a–c). According to DFT calculations, the Ov promoted the activation and dissociation of H_2O, which may lead to a H-rich surface and thus enhance the selectivity of C_{2+} products through the hydrogen-assisted coupling mechanism (Fig. 14d).

GB refers to the interface between crystal grains with different crystal orientations, a two-dimensional planar defect [158]. Introducing GBs to Cu-based catalysts can change the surface properties and reduce the reaction barrier [159,160]. Quantifying the role of GBs in Cu-catalyzed CO reduction is essential for establishing a firm design principle. As a typical work, Kanan's group [161] reported Cu NPs on carbon nanotubes (Cu/CNT) with different average GB densities (Fig. 14e), which exhibited a direct correlation between the activity of CO reduction to C_{2+} and GB densities. They used vapor deposition and thermal annealing to prepare Cu NPs on CNTs with different GB densities, and the GB densities were quantified by the length of the GBs and the particle area. With the increase in annealing temperature, a gradual decline in the GB densities was observed by TEM, leading to decrease of CO reduction activities and the FEs of C_{2+} products. The strong correlation between GB surface density and CO electroreduction activity suggests that GBs alter the surface properties of the particle to lower the barrier for this reaction. More recently, Niu *et al.* [75] reported a synthesis of Pb-Cu NPs with numerous Pb-concentrated GBs (Fig. 14f). It has been proposed that the "atomic size misfit" strategy can promote intra-lattice stress to induce and stabilize low-coordinated sites [162,163]. The Pb-Cu catalyst possesses abundant GBs compared with the Cu catalyst and a higher density of the Pb atoms are concentrated in the GBs zone, which reveals that the Pb-doping might be the main reason of the GB formation.

SFs is another type of planar defect that frequently manifests in metallic materials [164]. Wu *et al.* [65] reported a laser irradiation synthesis of $Cu_2(OH)_3NO_3$, as a precursor to make gerhardtite-derived Cu (GD-Cu) NPs with abundant SFs. It was discovered that the low coordination environment of SFs would upshift the Cu d-band center, leading to an increase d-electron back-donation to the CO 2π* antibonding orbital, thereby enhancing CO adsorption. An FE of 56% in CO-to-acetate electroreduction was achieved by regulating the *CO coverage in the GD-Cu with numerous defects. During the formation of SFs, there was a structural reconstruction of $Cu_2(OH)_3NO_3$ according to *ab initio* molecular dynamic (AIMD) simulations. The dynamic evolution of SFs was tracked in Fig. 14g, which exhibits disordered domains at 0.5 ps, and then these Cu atoms removed or inserted part of a close-packed layer of atoms forming SFs in the Cu crystal at 2 ps.

SYSTEMS DESIGN

Apart from catalyst materials, reaction environments also play an important role in modulating the ECOR performance [165,166]. The basic idea of system design is to create solid-liquid-gas triple-phase interfaces, which influences on the mass transport process in the gas-involved reaction [167]. In general, the improvement of ECOR system warrants consideration of catalyst support, cell configuration and gas diffusion electrode (GDE).

Catalyst support

At odds with electrocatalysts simply based on active compo-

© Science China Press 2024

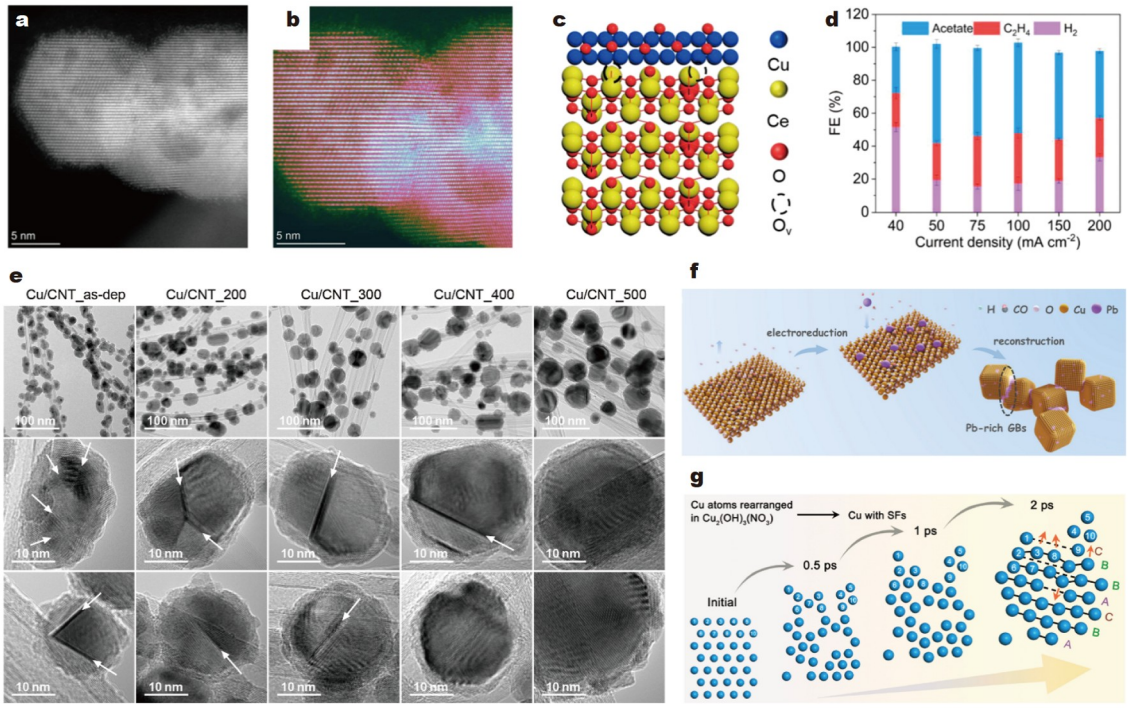

Figure 14 (a) Aberration-corrected HAADF-STEM (AC-HAADF-STEM) image, (b) colored AC-HAADF-STEM image, and (c) schematic model of Cu-CeO_2. (d) FEs of products on Cu-CeO_2. Reprinted with permission from Ref. [157], Copyright 2023, American Chemical Society. (e) TEM characterization of Cu NPs in the as-deposited Cu/CNT electrodes annealed under N_2 at 200, 300, 400 and 500°C. Reprinted with permission from Ref. [161], Copyright 2016, American Chemical Society. (f) Scheme of the synthesis of the Pb-Cu and the Cu electrocatalysts. Reprinted with permission from Ref. [75], Copyright 2023, The Author(s). (g) Dynamic evolution of SFs during the AIMD process. Part of atoms are numbered to track their movements. Reprinted with permission from Ref. [65], Copyright 2023, American Chemical Society.

nents, they might be highly dispersed on a support featured by adequate porosity and strong hydrophobicity for efficient mass transport and interface building [168,169]. By properly regulating the catalyst support, a superior catalytic performance could be achieved.

The hydrophobicity of the catalyst support is key in forming triple-phase boundaries and achieving high reaction rates [170,171]. Li *et al.* [49] prepared supported polycrystalline copper powder electrocatalysts by depositing those onto polytetrafluoroethylene (PTFE)-treated carbon fiber paper (Fig. 15a). Compared with that on non-PTFE-treated carbon fiber paper and glassy carbon, the Cu powder deposited on the PTFE treated hydrophobic carbon support showed the merit in improving the performance of CO electroreduction (Fig. 15b). More recently, Sargent's group [172] reported a carbon reservoir catalyst (CRC) (Fig. 15c), which incorporated Cu NPs into a microporous CO-capturing support to facilitate CO transport and distribution. Furthermore, by controlling the ratio of pyridinic and pyrrolic N atoms doped in the CRC, high ECOR selectivity to C_{2+} alcohols had been achieved at high carbon efficiency (Fig. 15d).

Besides, conductive polymers can be used to cover the surface of electrocatalysts to enrich intermediates, thereby promoting the selectivity toward C_{2+} products (Fig. 15e) [173]. Duan *et al.* [174] prepared the core-shell poly (ionic liquid)-Cu hybrids (Cu@PIL) by *in-situ* radical polymerization. As a result, Cu@PIL exhibited high C_{2+} selectivity and excellent tolerance across a broad range of CO concentrations. Remarkably, a high $FE_{C_{2+}}$ of 71.1% was achieved by feeding as less as 5.0 vol% CO (Fig. 15f). The performance was mainly attributed to the local enrichment of CO by the interaction with functionality at the PIL layer and the abundant porous structure of the skeleton enhancing the supply of CO to the active Cu@PIL interface, thereby enabling a specific CO-to-C_{2+} transformation.

Cell configuration

The ECOR is usually performed in flow cells, MEA cells, and H-cells. In a conventional H-cell (Fig. 16a), catalysts are deposited on carbon paper immersed in non-flowing electrolyte. Since feedstock gas is supplied from the bulk electrolyte, the reaction is mass transport limited, and the diffusion of gaseous reactants to the electrocatalyst is insufficient. More importantly, CO has low aqueous solubility, which further delays the reaction rate. Consequently, there are virtually no reports of employing H-cell in the research of ECOR.

In recent years, studies have switched to using flow-cells with GDEs, which allow for increased contact between the electrolyte, catalyst, and gas [175–177]. Jouny *et al.* [96] constructed a three-compartment CO flow cell where CO was directly fed on one side to the surface of catalyst while KOH electrolyte was fed on the other (Fig. 16b). The well-engineered triple-phase interface allowed remarkable CO-to-C_{2+} selectivity at high reaction rates. Furthermore, the MEA cell is an emerging platform that combines cathode:membrane:anode in a zero-gap configuration and reduces ohmic loss, liquid product losses and salt formation [178]. The cathode of an MEA cell does not need an electrolyte during operation, which results in better operational stability than that of a flow cell [179]. More recently, Hasa *et al.* [180] examined the role of membrane on product selectivity and cell stability in an MEA cell (Fig. 16c). They found that the prop-

 © Science China Press 2024

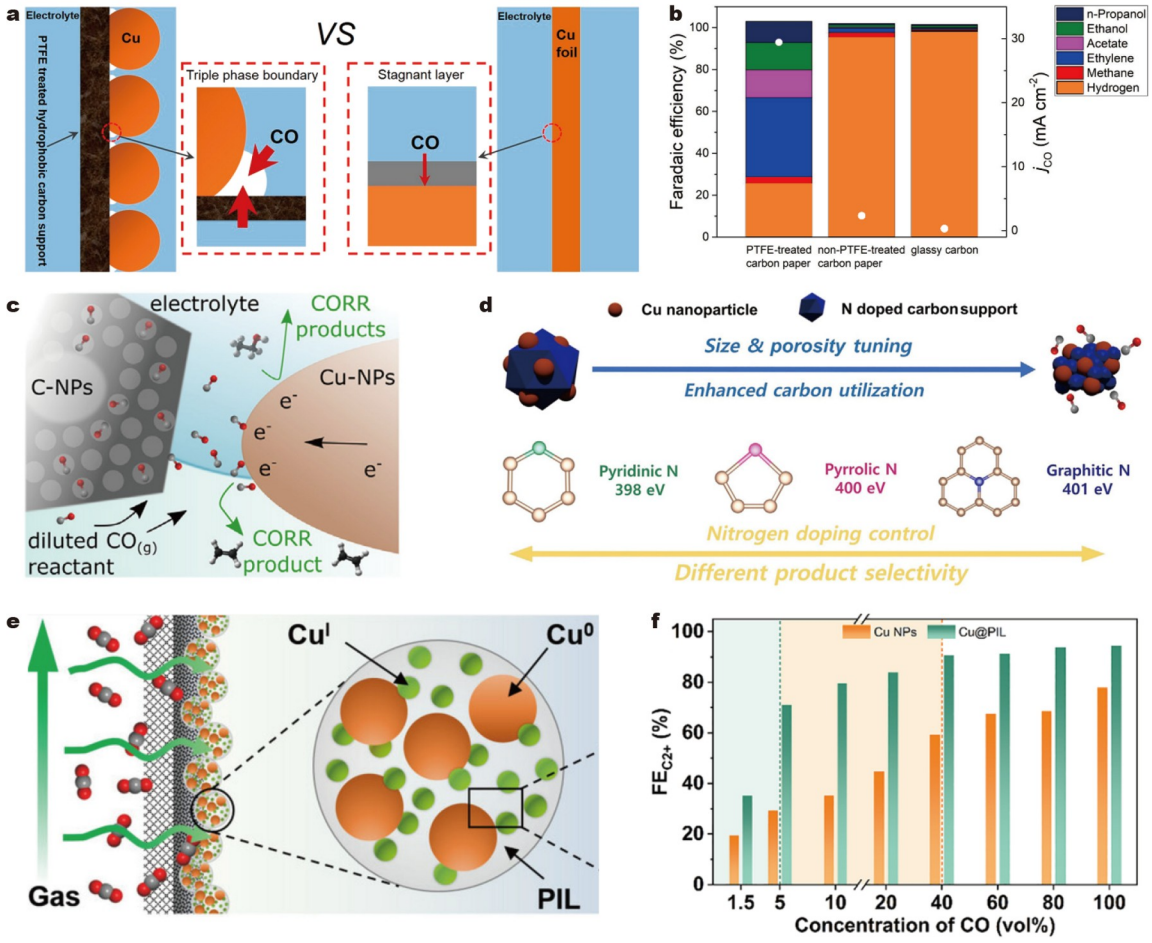

Figure 15 (a) CO mass transport at the carbon-supported electrode *vs.* the conventional electrode. (b) CO electrolysis results for different carbon supports. Reprinted with permission from Ref. [49], Copyright 2019, American Chemical Society. (c) CO availability in the gas phase electrolyzer when CO distribution is promoted at the catalytic active sites, CORR to desired C-products can occur at the diluted CO conditions. (d) Scheme of the different nitrogen groups in N-doped carbon support. Reprinted with permission from Ref. [172], Copyright 2023, Elsevier. (e) Scheme of a PIL-supported Cu-based catalyst. Reprinted with permission from Ref. [173], Copyright 2022, Wiley-VCH Verlag GmbH. (f) $FE_{C_{2+}}$ during CORR over Cu NPs and Cu@PIL with different concentrations of CO gas. Reprinted with permission from Ref. [174], Copyright 2023, Elsevier.

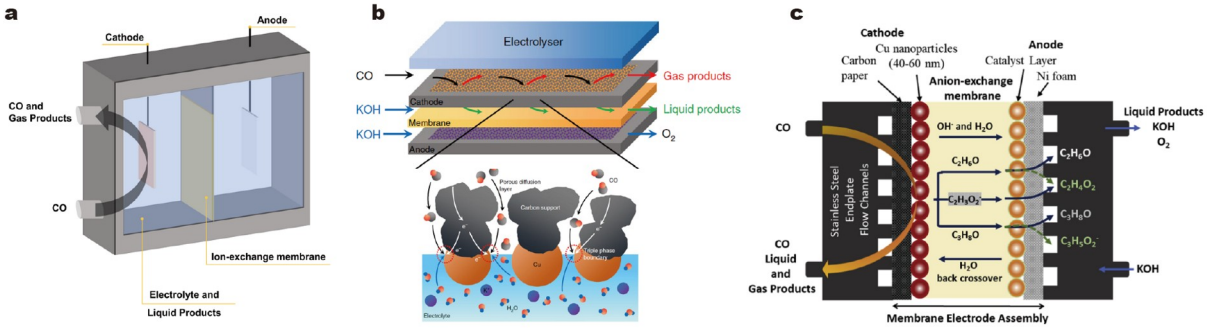

Figure 16 (a) Schematic illustration of H-cell. (b) Schematic illustration of flow cell. Reprinted with permission from Ref. [96], Copyright 2018, The Author (s). (c) Schematic illustration of MEA cell. Reprinted with permission from Ref. [180], Copyright 2023, Elsevier.

erties of the membrane significantly impacted the selectivity of the liquid product but had no impact on the gas products, because a high ethanol crossover through the membrane tuned the selectivity toward C_{2+} products.

GDE

The electrode structure plays the principal role in the reaction rate by supplying adequate gaseous reactants to the heterogeneous electrocatalyst surface [181]. The improvement of the ECOR reactor through electrode structure design based on GDE has been a hotpot in this field [182,183]. GDEs are high-surface-area, porous electrodes, consisting of catalyst layers and gas diffusion layer (GDL) supports [184]. The composition and structure of GDE can influence the transport of reactants and

© Science China Press 2024

products. For example, Xu *et al.* [185] proposed that cathodic GDE flooding and Ir contaminants are two main issues causing excessive HER during the testing period. PTFE is a hydrophobic polymer used to wet-proof GDLs and catalyst layers, which can effectively mitigate flooding. By increasing the PTFE content in the GDEs and using an alkaline stable Ni-based anode, these issues can be partly alleviated (Fig. 17a, b). However, high PTFE loadings (>15 wt%) might electrically insulate the catalyst layer and increase ohmic losses [186]. Therefore, methods that enable fine control over the hydrophobicity of GDEs are critical for striking this balance. On the other hand, the structure of GDE might influence the local environment of ECOR. Rabiee *et al.* [187] used hollow fiber GDEs (HFGDEs) with a nanocube copper layer for ECOR to C_{2+} products (Fig. 17c, d). Pushing CO through the hollow fiber porous wall into the electrolyte side likely led to a higher local CO concentration, more use of the catalytic active sites, and the formation of a triple-phase boundary.

SUMMARY AND OUTLOOK

The electroreduction of CO to value-added chemicals is an attractive technique to supplement the current FT synthesis and ECO_2R reaction. Through a cascade strategy to realize the utilization of CO_2, ECOR presents a higher selectivity to C_{2+} products. In this review, we have summarized the performance evaluation and the formation mechanisms of C_{2+} chemicals for ECOR reaction with focus on the Cu-based catalyst engineering and system design. A summary of the ECOR performance of various Cu-based electrocatalysts under different reaction conditions is given in Table 2. Although remarkable advances in the ECOR on Cu-based catalysts toward C_{2+} products have been achieved, several challenges are yet to be overcome and corresponding suggestions are listed in the following in terms of catalyst engineering and system design.

Catalyst engineering

In the plethora of research work reported at present, researchers often employ a trial-and-error synthesis strategy to screen efficient catalysts from a pool of candidate materials [188–192]. To address this issue, it is worth considering a theory-guided rational design. As of today, the application of DFT technology has shown great advantages in ECOR catalyst scrutiny and screening. Based on reaction descriptors such as binding strength, adsorption energy and Gibbs free energy, using DFT calculations can help to quantitatively describe and evaluate the performance of the catalyst [193–196]. Meanwhile, the reliability of the descriptors would require further research experimentally [197]. Such an approach enhances the efficiency of catalyst design, leading to greater selectivity, activity and stability.

Further effort is required to establish a good "structure-performance" correlation for efficient and real catalysts design. In addition to DFT calculations, with the joint help of various *in situ* characterization techniques, comprehensive studies can be carried out to disclose the complicated change in a real chemical environment, ranging from reaction intermediates to the structure, morphology and composition evolution at the elec-

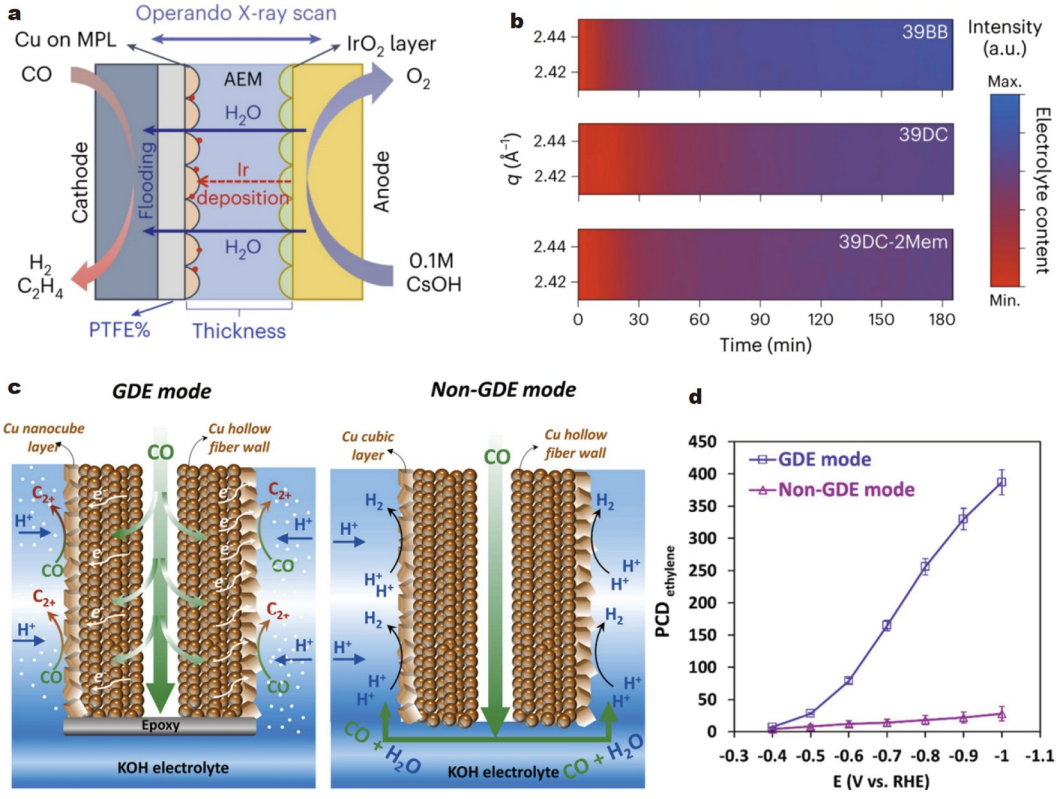

Figure 17 (a) Schematic diagram of the potential degradation mechanism of the MEA during ECOR. (b) *Operando* wide-angle X-ray scattering (WAXS) mappings at the region of MPL. Reprinted with permission from Ref. [185], Copyright 2023, The Author(s). (c) Schematic of CO delivery mechanisms in GDE and non-GDE mode. In GDE mode the HFGDEs are dead-end, and therefore CO diffuses through the hollow fiber walls under pressure. (d) Partial current density of ethylene formation on CuCube HFGDE as a function of the applied potentials in GDE and non-GDE mode. Reprinted with permission from Ref. [187], Copyright 2023, Elsevier.

© Science China Press 2024

Table 2 Summary of relevant Cu-based catalysts with doping and alloying, morphology control, surface modification, *in situ* reconstruction, or defect engineering for ECOR

Catalysts	Electrolyte	Applied conditions	FE (%)					Ref.
			C_2H_4	C_2H_5OH	CH_3COO^-	n-C_3H_7OH	C_{2+}	
Ag-Cu_2O	1.0 M KOH	200 mA cm^{-2}	~25	~2	~70	–	–	[112]
$Cu(OD)_{0.8}Ag_{0.2}$	1.0 M KOH	−0.56 V *vs.* RHE	13.3	–	–	–	76.9	[113]
Cu/Ag-DA	5.0 M KOH	−0.57 V *vs.* RHE	5.2	1.8	91.2	–	–	[57]
Cu-Pd	1.0 M KOH	−1.0 V *vs.* RHE	–	–	65	–	~72	[115]
Pd-doped Cu	1.0 M KOH	−0.62 V *vs.* RHE	37	39.5	–	–	–	[111]
CuPd	1.0 M KOH	−0.84 V *vs.* RHE	~18	~8	~54	~5	–	[116]
Cu-Au	1.0 M KOH	700 mA cm^{-2}	6.97	7.02	31.01	–	45	[94]
Ag-Ru-Cu	1.0 M KOH	300 mA cm^{-2}	28.9	16	6.6	37	90	[119]
Cu nanowire	0.1 M KOH	−0.3 V *vs.* RHE	0.66	49.79	14.50	–	–	[126]
Triangular Cu nanosheets	2.0 M KOH	−0.63 V *vs.* RHE	16.3	2.4	48	2.0	68.7	[127]
Fragmented Cu	1.0 M KOH	−0.45 V *vs.* RHE	~23	~17	~5	20.3	~65	[98]
Cu nanocavity	1.0 M KOH	−0.56 V *vs.* RHE	21	12.5	7.8	21	62.3	[100]
$(Cu_2O@)_2Cu_2O$	1.0 M KOH	50 mA cm^{-2}	~20	~15	~10	22.22	~73	[128]
BCF-Cu_2O	1.0 M KOH	−0.45 V *vs.* RHE	24	13	26	15	84	[60]
Cu-Ppy	1.0 M KOH	−0.78 V *vs.* RHE	69	~10	~12	–	–	[131]
Cu CP	3.0 M KOH	−0.59 V *vs.* RHE	~10	–	61	–	~70	[62]
Cu@NH_2	1.0 M KOH	−0.75 V *vs.* RHE	~20	~18	51.5	–	~70	[132]
R-Cu/Au	1.0 M KOH	−0.58 V *vs.* RHE	~15	~20	–	46.6	–	[147]
$Ag_2Cu_2O_3$	1.0 M $CsHCO_3$	−0.83 V *vs.* RHE	~25	~34	~25	~8	~92	[148]
CuTCNQ	1.0 M KOH	−0.69 V *vs.* RHE	~28	~12	39.9	–	81.3	[63]
CuPc	1.0 M KOH	700 mA cm^{-2}	~20	~10	~50	~8	–	[149]
Cu-CeO_2	1.0 M KOH	50 mA cm^{-2}	~20	–	~60	–	–	[157]
Cu/CNT	0.1 M KOH	−0.3 V *vs.* RHE	–	37	35	–	–	[161]
Pd-Cu	1.0 M KOH	−0.68 V *vs.* RHE	13.4	20	10	46.6	–	[75]
GD-Cu	3.0 M KOH	400 mA cm^{-2}	~16	~14	~56	–	~85	[65]

trode scale. Advanced *in situ* characterization technology such as *operando* scanning tunneling microscope, *operando* TEM, *operando* SEM, and *operando* XRD, would provide helpful information for revealing the reaction pathways under realistic reaction conditions. These days, *in situ* surface-enhanced Raman spectroscopy (SERS) and *in situ* SEIRAS are used to provide direct evidence substantially enhanced intermediates enrichment on Cu-based catalysts [198–200]. From the perspective of practical application, catalysts often cannot be directly scaled up for production. Therefore, developing advanced catalyst preparation techniques is also a crucial direction for the future.

System design

To date, the formation of the C_{2+} products is still far from commercialization [36,142,201–205]. Due to the insufficient intrinsic activity of catalyst materials, as well as the competition for protons with hydrogen evolution reaction in aqueous solvents, there still remains a demand for a large overpotential to deliver appreciable current. Therefore, the effective modification of catalyst materials and the reaction environment will help improve the kinetics of the ECOR process. Catalyst development strategies of increasing both intrinsic activity and number of active sites can be further explored based on that mentioned in this review. Moreover, CO_2 electroreduction in strongly acidic medium has been demonstrated to have lower overall cell voltage than that with the near-neutral and alkaline media [206–208]. However, there is a dearth of research on electrochemical reduction of carbon monoxide under acidic conditions, and there is significant scope for improvement in this field [209]. If low overpotential, high current density, and long-term stability can be achieved in the ECOR reaction, and if it can work in cooperation with ECO_2R, the utilization of CO_2 driven by electrocatalysis will accelerate its approach to carbon-neutral applications.

Another huge barrier for commercialization is the lower carbon efficiency. Although ECOR can address carbon losses from carbonate formation in alkaline solution, only a small portion of feedstock gas is converted to desirable products, while a large amount of unreacted CO gas escapes. Accordingly, the development of gas circulating system is necessary to enhance the

© Science China Press 2024

feedstock gas usage. By reducing the carbon monoxide content in the feed gas, carbon efficiency can be significantly improved. Unfortunately, almost all ECOR systems reported in current research employ pure CO as their feedstock. This is grossly incompatible with practical application scenarios and further restricts the utilization of mixed gas produced by a single-pass ECOR process. Therefore, more efforts should be devoted to the research of impure CO process feeds theoretically and experimentally.

ECOR technology is an emerging platform for artificial carbon fixation, and there are many challenges and opportunities in the development of this field. This review offers guidance for the rational design of Cu-based catalysts for ECOR. From industrial consideration, we also expect to develop more copper-based catalysts with superior performance to facilitate the transition from lab-scale discoveries to industrial-scale set-up in the future.

Received 27 December 2023; accepted 19 March 2024; published online 13 May 2024

1 Birdja YY, Pérez-Gallent E, Figueiredo MC, *et al.* Advances and challenges in understanding the electrocatalytic conversion of carbon dioxide to fuels. Nat Energy, 2019, 4: 732–745
2 Wang Y, Liu J, Zheng G. Designing copper-based catalysts for efficient carbon dioxide electroreduction. Adv Mater, 2021, 33: 2005798
3 Zheng Y, Vasileff A, Zhou X, *et al.* Understanding the roadmap for electrochemical reduction of CO_2 to multi-carbon oxygenates and hydrocarbons on copper-based catalysts. J Am Chem Soc, 2019, 141: 7646–7659
4 Nitopi S, Bertheussen E, Scott SB, *et al.* Progress and perspectives of electrochemical CO_2 reduction on copper in aqueous electrolyte. Chem Rev, 2019, 119: 7610–7672
5 Fu J, Li P, Lin Y, *et al.* Fight for carbon neutrality with state-of-the-art negative carbon emission technologies. Eco-Environ Health, 2022, 1: 259–279
6 Liu J, Zhu C, Liu X, *et al.* Nonmicrobial mechanisms dominate the release of CO_2 and the decomposition of organic matter during the short-term redox process in paddy soil slurry. Eco-Environ Health, 2023, 2: 227–234
7 Zaidi SAH, Hussain M, Uz Zaman Q. Dynamic linkages between financial inclusion and carbon emissions: Evidence from selected OECD countries. Resources Environ Sustainability, 2021, 4: 100022
8 Wang F, Liu J, Qin G, *et al.* Coastal blue carbon in China as a nature-based solution toward carbon neutrality. Innovation, 2023, 4: 100481
9 Hui S, Jiang Y, Jiang Y, *et al.* Cathode materials in microbial electrosynthesis systems for carbon dioxide reduction: Recent progress and perspectives. Energy Mater, 2023, 3: 300055
10 Chen JM. Carbon neutrality: Toward a sustainable future. Innovation, 2021, 2: 100127
11 Wang F, Harindintwali JD, Yuan Z, *et al.* Technologies and perspectives for achieving carbon neutrality. Innovation, 2021, 2: 100180
12 Jiang Y, Tian S, Li H, *et al.* Harnessing microbial electrosynthesis for a sustainable future. TIMS, 2023, 1: 100008
13 Cao C, Zhou S, Zuo S, *et al.* Si doping-induced electronic structure regulation of single-atom Fe sites for boosted CO_2 electroreduction at low overpotentials. Research, 2023, 6: 0079
14 Zhu W, Fu J, Liu J, *et al.* Tuning single atom-nanoparticle ratios of Ni-based catalysts for synthesis gas production from CO_2. Appl Catal B-Environ, 2020, 264: 118502
15 Liu LX, Zhou Y, Chang YC, *et al.* Tuning Sn_3O_4 for CO_2 reduction to formate with ultra-high current density. Nano Energy, 2020, 77: 105296
16 Zhu W, Michalsky R, Metin Ö, *et al.* Monodisperse Au nanoparticles for selective electrocatalytic reduction of CO_2 to CO. J Am Chem Soc, 2013, 135: 16833–16836
17 Masood ul Hasan I, Peng L, Mao J, *et al.* Carbon-based metal-free catalysts for electrochemical CO_2 reduction: Activity, selectivity, and stability. Carbon Energy, 2021, 3: 24–49
18 Li X, Chen Y, Zhan X, *et al.* Strategies for enhancing electrochemical CO_2 reduction to multi-carbon fuels on copper. TIMS, 2023, 1: 100014
19 Wu Y, Du H, Li P, *et al.* Heterogeneous electrocatalysis of carbon dioxide to methane. Methane, 2023, 2: 148–175
20 Wang X, Li P, Cao Y, *et al.* Techno-economic analysis and industrial application prospects of single-atom materials in CO_2 catalysis. Chem J Chin U, 2022, 43: 20220347
21 Ross MB, De Luna P, Li Y, *et al.* Designing materials for electrochemical carbon dioxide recycling. Nat Catal, 2019, 2: 648–658
22 Lu X, Tong D, He K. China's carbon neutrality: An extensive and profound systemic reform. Front Environ Sci Eng, 2023, 17: 14
23 Yang H, Huang X, Hu J, *et al.* Achievements, challenges and global implications of China's carbon neutral pledge. Front Environ Sci Eng, 2022, 16: 111
24 Li L, Zhao ZJ, Zhang G, *et al.* Neural network accelerated investigation of the dynamic structure–performance relations of electrochemical CO_2 reduction over SnO_x surfaces. Research, 2023, 6: 0067
25 Dinh CT, García de Arquer FP, Sinton D, *et al.* High rate, selective, and stable electroreduction of CO_2 to CO in basic and neutral media. ACS Energy Lett, 2018, 3: 2835–2840
26 Kim JYT, Zhu P, Chen FY, *et al.* Recovering carbon losses in CO_2 electrolysis using a solid electrolyte reactor. Nat Catal, 2022, 5: 288–299
27 Xie L, Jiang Y, Zhu W, *et al.* Cu-based catalyst designs in CO_2 electroreduction: Precise modulation of reaction intermediates for high-value chemical generation. Chem Sci, 2023, 14: 13629–13660
28 Zhu W, Zhang YJ, Zhang H, *et al.* Active and selective conversion of CO_2 to CO on ultrathin Au nanowires. J Am Chem Soc, 2014, 136: 16132–16135
29 Cai Y, Fu J, Zhou Y, *et al.* Insights on forming N,O-coordinated Cu single-atom catalysts for electrochemical reduction CO_2 to methane. Nat Commun, 2021, 12: 586
30 Cho JH, Ma J, Kim SY. Toward high-efficiency photovoltaics-assisted electrochemical and photoelectrochemical CO_2 reduction: Strategy and challenge. Exploration, 2023, 3: 20230001
31 Zhu F, Ge J, Gao Y, *et al.* Molten salt electro-preparation of graphitic carbons. Exploration, 2023, 3: 20210186
32 Jin S, Hao Z, Zhang K, *et al.* Advances and challenges for the electrochemical reduction of CO_2 to CO: From fundamentals to industrialization. Angew Chem Int Ed, 2021, 60: 20627–20648
33 Chen Z, Wang C, Zhong X, *et al.* Achieving efficient CO_2 electrolysis to CO by local coordination manipulation of nickel single-atom catalysts. Nano Lett, 2023, 23: 7046–7053
34 Zhu W, Kattel S, Jiao F, *et al.* Shape-controlled CO_2 electrochemical reduction on nanosized Pd hydride cubes and octahedra. Adv Energy Mater, 2019, 9: 1802840
35 Song RB, Zhu W, Fu J, *et al.* Electrode materials engineering in electrocatalytic CO_2 reduction: Energy input and conversion efficiency. Adv Mater, 2020, 32: 1903796
36 Chen Y, Zhang J, Yang L, *et al.* Recent advances in non-precious metal–nitrogen–carbon single-site catalysts for CO_2 electroreduction reaction to CO. Electrochem Energy Rev, 2022, 5: 11
37 Nguyen DLT, Kim Y, Hwang YJ, *et al.* Progress in development of electrocatalyst for CO_2 conversion to selective CO production. Carbon Energy, 2020, 2: 72–98
38 Yan C, Yuan H, Wang X, *et al.* Sn-doping stabilizes residual oxygen species to promote intermediate desorption for enhanced CO_2 to CO conversion. Sci China Mater, 2023, 66: 3547–3554
39 Jiao F, Li J, Pan X, *et al.* Selective conversion of syngas to light olefins. Science, 2016, 351: 1065–1068
40 Xu M, Qin X, Xu Y, *et al.* Boosting CO hydrogenation towards C_{2+} hydrocarbons over interfacial TiO_{2-x}/Ni catalysts. Nat Commun, 2022, 13: 6720
41 Liang X, Meng X, Yang J, *et al.* Liquid viscosity and density of squalane and squalane with dissolved carbon dioxide at temperatures from (298.15 to 548.15) K. Int J Thermophys, 2023, 44: 168
42 Zhou W, Cheng K, Kang J, *et al.* New horizon in C1 chemistry: Breaking the selectivity limitation in transformation of syngas and

 © Science China Press 2024

hydrogenation of CO_2 into hydrocarbon chemicals and fuels. Chem Soc Rev, 2019, 48: 3193–3228
43 Wentrup J, Pesch GR, Thöming J. Dynamic operation of Fischer-Tropsch reactors for power-to-liquid concepts: A review. Renew Sustain Energy Rev, 2022, 162: 112454
44 Wu HK, Zhang F, Li JY, *et al.* Photo-driven Fischer–Tropsch synthesis. J Mater Chem A, 2020, 8: 24253–24266
45 Du H, Fu J, Liu LX, *et al.* Recent progress in electrochemical reduction of carbon monoxide toward multi-carbon products. Mater Today, 2022, 59: 182–199
46 Kim JYT, Sellers C, Hao S, *et al.* Different distributions of multi-carbon products in CO_2 and CO electroreduction under practical reaction conditions. Nat Catal, 2023, 6: 1115–1124
47 Jouny M, Hutchings GS, Jiao F. Carbon monoxide electroreduction as an emerging platform for carbon utilization. Nat Catal, 2019, 2: 1062–1070
48 Overa S, Crandall BS, Shrimant B, *et al.* Enhancing acetate selectivity by coupling anodic oxidation to carbon monoxide electroreduction. Nat Catal, 2022, 5: 738–745
49 Li J, Chang K, Zhang H, *et al.* Effectively increased efficiency for electroreduction of carbon monoxide using supported polycrystalline copper powder electrocatalysts. ACS Catal, 2019, 9: 4709–4718
50 Ma M, Deng W, Xu A, *et al.* Local reaction environment for selective electroreduction of carbon monoxide. Energy Environ Sci, 2022, 15: 2470–2478
51 Ozden A, García de Arquer FP, Huang JE, *et al.* Carbon-efficient carbon dioxide electrolysers. Nat Sustain, 2022, 5: 563–573
52 Yu SH, Antonietti M. Creative and relevant materials innovation. TIMS, 2023, 1: 100002
53 Xiang Y, Sun Y, Liu Y, *et al.* Computational design of a two-dimensional copper carbide monolayer as a highly efficient catalyst for carbon monoxide electroreduction to ethanol. ACS Appl Mater Interfaces, 2023, 15: 13033–13041
54 Ji Y, Guan A, Zheng G. Copper-based catalysts for electrochemical carbon monoxide reduction. Cell Rep Phys Sci, 2022, 3: 101072
55 Zhang H, Li J, Cheng MJ, *et al.* CO electroreduction: Current development and understanding of Cu-based catalysts. ACS Catal, 2019, 9: 49–65
56 Yu J, Wang J, Ma Y, *et al.* Recent progresses in electrochemical carbon dioxide reduction on copper-based catalysts toward multicarbon products. Adv Funct Mater, 2021, 31: 2102151
57 Jin J, Wicks J, Min Q, *et al.* Constrained C_2 adsorbate orientation enables CO-to-acetate electroreduction. Nature, 2023, 617: 724–729
58 Gao A, Gu L. Insight into materials science from a reductionist perspective. TIMS, 2023, 1: 100009
59 Duong HP, Rivera de la Cruz JG, Tran NH, *et al.* Silver and copper nitride cooperate for CO electroreduction to propanol. Angew Chem Int Ed, 2023, 62: e202310788
60 Liu J, You F, He B, *et al.* Directing the architecture of surface-clean Cu_2O for CO electroreduction. J Am Chem Soc, 2022, 144: 12410–12420
61 Shi Q, Zhu W, Zhong H, *et al.* Highly dispersed platinum atoms on the surface of AuCu metallic aerogels for enabling H_2O_2 production. ACS Appl Energy Mater, 2019, 2: 7722–7727
62 Luo M, Ozden A, Wang Z, *et al.* Coordination polymer electrocatalysts enable efficient CO-to-acetate conversion. Adv Mater, 2023, 35: 2209567
63 Du H, Liu LX, Cai Y, *et al. In situ* formed N-containing copper nanoparticles: A high-performance catalyst toward carbon monoxide electroreduction to multicarbon products with high faradaic efficiency and current density. Nanoscale, 2022, 14: 7262–7268
64 Lai J, Zhang Z, Yang> X, *et al.* Opening the black box: Insights into the restructuring mechanism to steer catalytic performance. TIMS, 2023, 1: 100020
65 Wu ZZ, Zhang XL, Yang PP, *et al.* Gerhardtite as a precursor to an efficient CO-to-acetate electroreduction catalyst. J Am Chem Soc, 2023, 145: 24338–24348
66 Hou J, Chang X, Li J, *et al.* Correlating CO coverage and CO electroreduction on Cu *via* high-pressure *in situ* spectroscopic and reactivity investigations. J Am Chem Soc, 2022, 144: 22202–22211
67 Yang W, Liu H, Qi Y, *et al.* Boosting C–C coupling to multicarbon products *via* high-pressure CO electroreduction. J Energy Chem, 2023, 85: 102–107
68 Du J, Chen A, Hou S, *et al.* CNT modified by mesoporous carbon anchored by Ni nanoparticles for CO_2 electrochemical reduction. Carbon Energy, 2022, 4: 1274–1284
69 Ruqia B, Tomboc GM, Kwon T, *et al.* Recent advances in the electrochemical CO reduction reaction towards highly selective formation of C_X products (X = 1–3). Chem Catal, 2022, 2: 1961–1988
70 De Luna P, Hahn C, Higgins D, *et al.* What would it take for renewably powered electrosynthesis to displace petrochemical processes? Science, 2019, 364: eaav3506
71 Yi JD, Gao X, Zhou H, *et al.* Design of Co-Cu diatomic site catalysts for high-efficiency synergistic CO_2 electroreduction at industrial-level current density. Angew Chem Int Ed, 2022, 61: e202212329
72 Martín AJ, Larrazábal GO, Pérez-Ramírez J. Towards sustainable fuels and chemicals through the electrochemical reduction of CO_2: Lessons from water electrolysis. Green Chem, 2015, 17: 5114–5130
73 Li J, Wang Z, McCallum C, *et al.* Constraining CO coverage on copper promotes high-efficiency ethylene electroproduction. Nat Catal, 2019, 2: 1124–1131
74 Ma G, Syzgantseva OA, Huang Y, *et al.* A hydrophobic Cu/Cu_2O sheet catalyst for selective electroreduction of CO to ethanol. Nat Commun, 2023, 14: 501
75 Niu W, Chen Z, Guo W, *et al.* Pb-rich Cu grain boundary sites for selective CO-to-*n*-propanol electroconversion. Nat Commun, 2023, 14: 4882
76 Yin Z, Peng H, Wei X, *et al.* An alkaline polymer electrolyte CO_2 electrolyzer operated with pure water. Energy Environ Sci, 2019, 12: 2455–2462
77 Lagadec MF, Grimaud A. Water electrolysers with closed and open electrochemical systems. Nat Mater, 2020, 19: 1140–1150
78 Möller T, Ju W, Bagger A, *et al.* Efficient CO_2 to CO electrolysis on solid Ni–N–C catalysts at industrial current densities. Energy Environ Sci, 2019, 12: 640–647
79 Wei P, Li H, Lin L, *et al.* CO_2 electrolysis at industrial current densities using anion exchange membrane based electrolyzers. Sci China Chem, 2020, 63: 1711–1715
80 She X, Wang Y, Xu H, *et al.* Challenges and opportunities in electrocatalytic CO_2 reduction to chemicals and fuels. Angew Chem Int Ed, 2022, 61: e202211396
81 Xiang SQ, Shi JL, Gao ST, *et al.* Thermodynamic and kinetic competition between C–H and O–H bond formation pathways during electrochemical reduction of CO on copper electrodes. ACS Catal, 2021, 11: 2422–2434
82 Montoya JH, Shi C, Chan K, *et al.* Theoretical insights into a CO dimerization mechanism in CO_2 electroreduction. J Phys Chem Lett, 2015, 6: 2032–2037
83 Goodpaster JD, Bell AT, Head-Gordon M. Identification of possible pathways for C–C bond formation during electrochemical reduction of CO_2 : New theoretical insights from an improved electrochemical model. J Phys Chem Lett, 2016, 7: 1471–1477
84 Garza AJ, Bell AT, Head-Gordon M. Mechanism of CO_2 reduction at copper surfaces: Pathways to C_2 products. ACS Catal, 2018, 8: 1490–1499
85 Wang L, Nitopi SA, Bertheussen E, *et al.* Electrochemical carbon monoxide reduction on polycrystalline copper: Effects of potential, pressure, and pH on selectivity toward multicarbon and oxygenated products. ACS Catal, 2018, 8: 7445–7454
86 Lin Y, Wang T, Zhang L, *et al.* Tunable CO_2 electroreduction to ethanol and ethylene with controllable interfacial wettability. Nat Commun, 2023, 14: 3575
87 Ma W, Xie S, Liu T, *et al.* Electrocatalytic reduction of CO_2 to ethylene and ethanol through hydrogen-assisted C–C coupling over fluorine-modified copper. Nat Catal, 2020, 3: 478–487
88 Cheng T, Xiao H, Goddard WA. Nature of the active sites for CO reduction on copper nanoparticles; suggestions for optimizing performance. J Am Chem Soc, 2017, 139: 11642–11645

 © Science China Press 2024

89 Pérez-Gallent E, Figueiredo MC, Calle-Vallejo F, *et al.* Spectroscopic observation of a hydrogenated CO dimer intermediate during CO reduction on Cu(100) electrodes. Angew Chem Int Ed, 2017, 56: 3621–3624
90 Calle-Vallejo F, Koper MTM. Theoretical considerations on the electroreduction of CO to C_2 species on Cu(100) electrodes. Angew Chem Int Ed, 2013, 52: 7282–7285
91 Chen R, Su H, Liu D, *et al.* Highly selective production of ethylene by the electroreduction of carbon monoxide. Angew Chem Int Ed, 2020, 59: 154–160
92 Lum Y, Cheng T, Goddard Iii WA, *et al.* Electrochemical CO reduction builds solvent water into oxygenate products. J Am Chem Soc, 2018, 140: 9337–9340
93 Ni F, Yang H, Wen Y, *et al.* N-modulated Cu^+ for efficient electrochemical carbon monoxide reduction to acetate. Sci China Mater, 2020, 63: 2606–2612
94 Sun Q, Zhao Y, Tan X, *et al.* Atomically dispersed Cu–Au alloy for efficient electrocatalytic reduction of carbon monoxide to acetate. ACS Catal, 2023, 13: 5689–5696
95 Jouny M, Lv JJ, Cheng T, *et al.* Formation of carbon–nitrogen bonds in carbon monoxide electrolysis. Nat Chem, 2019, 11: 846–851
96 Jouny M, Luc W, Jiao F. High-rate electroreduction of carbon monoxide to multi-carbon products. Nat Catal, 2018, 1: 748–755
97 Wei P, Gao D, Liu T, *et al.* Coverage-driven selectivity switch from ethylene to acetate in high-rate CO_2/CO electrolysis. Nat Nanotechnol, 2023, 18: 299–306
98 Pang Y, Li J, Wang Z, *et al.* Efficient electrocatalytic conversion of carbon monoxide to propanol using fragmented copper. Nat Catal, 2019, 2: 251–258
99 Xiao H, Cheng T, Goddard Iii WA. Atomistic mechanisms underlying selectivities in C_1 and C_2 products from electrochemical reduction of CO on Cu(111). J Am Chem Soc, 2017, 139: 130–136
100 Zhuang TT, Pang Y, Liang ZQ, *et al.* Copper nanocavities confine intermediates for efficient electrosynthesis of C_3 alcohol fuels from carbon monoxide. Nat Catal, 2018, 1: 946–951
101 Liu C, Zhang M, Li J, *et al.* Nanoconfinement engineering over hollow multi-shell structured copper towards efficient electrocatalytical C–C coupling. Angew Chem Int Ed, 2022, 61: e202113498
102 Du M, Li X, Pang H, *et al.* Alloy electrocatalysts. EnergyChem, 2023, 5: 100083
103 Zhu W, Tackett BM, Chen JG, *et al.* Bimetallic electrocatalysts for CO_2 reduction. Top Curr Chem (Z), 2018, 376: 41
104 Zhang J, Yu P, Peng C, *et al.* Efficient CO electroreduction to methanol by CuRh alloys with isolated Rh sites. ACS Catal, 2023, 13: 7170–7177
105 Chen T, Liu T, Shen X, *et al.* Synergistically electronic tuning of metalloid CdSe nanorods for enhanced electrochemical CO_2 reduction. Sci China Mater, 2021, 64: 2997–3006
106 Zhang J, Sui R, Xue Y, *et al.* Direct synthesis of parallel doped N-MoP/N-CNT as highly active hydrogen evolution reaction catalyst. Sci China Mater, 2019, 62: 690–698
107 Zhou Y, Zhou Z, Chen M, *et al.* Doping and alloying for improved perovskite solar cells. J Mater Chem A, 2016, 4: 17623–17635
108 Huang H, Jia H, Liu Z, *et al.* Understanding of strain effects in the electrochemical reduction of CO_2: Using Pd nanostructures as an ideal platform. Angew Chem Int Ed, 2017, 56: 3594–3598
109 Wang L, Higgins DC, Ji Y, *et al.* Selective reduction of CO to acetaldehyde with CuAg electrocatalysts. Proc Natl Acad Sci USA, 2020, 117: 12572–12575
110 Wang X, Wang Z, Zhuang TT, *et al.* Efficient upgrading of CO to C_3 fuel using asymmetric C–C coupling active sites. Nat Commun, 2019, 10: 5186
111 Li J, Xu A, Li F, *et al.* Enhanced multi-carbon alcohol electroproduction from CO *via* modulated hydrogen adsorption. Nat Commun, 2020, 11: 3685
112 Dorakhan R, Grigioni I, Lee BH, *et al.* A silver–copper oxide catalyst for acetate electrosynthesis from carbon monoxide. Nat Synth, 2023, 2: 448–457
113 Li J, Xiong H, Liu X, *et al.* Weak CO binding sites induced by Cu–Ag interfaces promote CO electroreduction to multi-carbon liquid products. Nat Commun, 2023, 14: 698
114 Mu Z, Han N, Xu D, *et al.* Critical role of hydrogen sorption kinetics in electrocatalytic CO_2 reduction revealed by on-chip *in situ* transport investigations. Nat Commun, 2022, 13: 6911
115 Shen H, Wang Y, Chakraborty T, *et al.* Asymmetrical C–C coupling for electroreduction of CO on bimetallic Cu–Pd catalysts. ACS Catal, 2022, 12: 5275–5283
116 Ji Y, Chen Z, Wei R, *et al.* Selective CO-to-acetate electroreduction *via* intermediate adsorption tuning on ordered Cu–Pd sites. Nat Catal, 2022, 5: 251–258
117 Nørskov JK, Bligaard T, Rossmeisl J, *et al.* Towards the computational design of solid catalysts. Nat Chem, 2009, 1: 37–46
118 Yuan X, Zhang L, Li L, *et al.* Ultrathin Pd–Au shells with controllable alloying degree on Pd nanocubes toward carbon dioxide reduction. J Am Chem Soc, 2019, 141: 4791–4794
119 Wang X, Ou P, Ozden A, *et al.* Efficient electrosynthesis of *n*-propanol from carbon monoxide using a Ag–Ru–Cu catalyst. Nat Energy, 2022, 7: 170–176
120 Dong H, Zhang X, Li J, *et al.* Construction of morphology-controlled nonmetal 2D/3D homojunction towards enhancing photocatalytic activity and mechanism insight. Appl Catal B-Environ, 2020, 263: 118270
121 Shakeel M, Arif M, Yasin G, *et al.* Layered by layered Ni-Mn-LDH/g-C_3N_4 nanohybrid for multi-purpose photo/electrocatalysis: Morphology controlled strategy for effective charge carriers separation. Appl Catal B-Environ, 2019, 242: 485–498
122 Hu Q, Qin Y, Wang X, *et al.* Reaction intermediate-mediated electrocatalyst synthesis favors specified facet and defect exposure for efficient nitrate–ammonia conversion. Energy Environ Sci, 2021, 14: 4989–4997
123 Meng X, Yang Y, Chen L, *et al.* A control over hydrogenation selectivity of furfural *via* tuning exposed facet of Ni catalysts. ACS Catal, 2019, 9: 4226–4235
124 Zhang M, Xiao C, Yan X, *et al.* Efficient removal of organic pollutants by metal–organic framework derived Co/C yolk–shell nanoreactors: Size-exclusion and confinement effect. Environ Sci Technol, 2020, 54: 10289–10300
125 Liu W, Qi J, Bai P, *et al.* Utilizing spatial confinement effect of N atoms in micropores of coal-based metal-free material for efficiently electrochemical reduction of carbon dioxide. Appl Catal B-Environ, 2020, 272: 118974
126 Raciti D, Cao L, Livi KJT, *et al.* Low-overpotential electroreduction of carbon monoxide using copper nanowires. ACS Catal, 2017, 7: 4467–4472
127 Luc W, Fu X, Shi J, *et al.* Two-dimensional copper nanosheets for electrochemical reduction of carbon monoxide to acetate. Nat Catal, 2019, 2: 423–430
128 Du H, Liu LX, Li P, *et al.* Enriching reaction intermediates in multi-shell structured copper catalysts for boosted propanol electrosynthesis from carbon monoxide. ACS Nano, 2023, 17: 8663–8670
129 Li F, Thevenon A, Rosas-Hernández A, *et al.* Molecular tuning of CO_2-to-ethylene conversion. Nature, 2020, 577: 509–513
130 Zhou X, Shan J, Zheng M, *et al.* Tuning molecular electrophilicity on Cu catalysts to steer CO_2 electroreduction selectivity. Sci China Mater, 2023, doi: 10.1007/s40843-023-2676-y
131 Ji Y, Yang C, Qian L, *et al.* Promoting electrocatalytic carbon monoxide reduction to ethylene on copper-polypyrrole interface. J Colloid Interface Sci, 2021, 600: 847–853
132 Wang Y, Zhao J, Cao C, *et al.* Amino-functionalized Cu for efficient electrochemical reduction of CO to acetate. ACS Catal, 2023, 13: 3532–3540
133 Piqué O, Viñes F, Illas F, *et al.* Elucidating the structure of ethanol-producing active sites at oxide-derived Cu electrocatalysts. ACS Catal, 2020, 10: 10488–10494
134 Obasanjo CA, Zeraati AS, Shiran HS, *et al. In situ* regeneration of copper catalysts for long-term electrochemical CO_2 reduction to multiple carbon products. J Mater Chem A, 2022, 10: 20059–20070
135 Hu Y, Wang X, Zhang J, *et al. In situ* engineering 3D conductive core-

 © Science China Press 2024

shell nano-networks and electronic structure of bismuth alloy nanosheets for efficient electrocatalytic CO_2 reduction. Sci China Mater, 2023, 66: 2266–2273
136 Zhao Q, Wang J, Zhuang Y, *et al.* *In situ* reconstruction of Bi nanoparticles confined within 3D nanoporous Cu to boost CO_2 electroreduction. Sci China Mater, 2024, 67: 796–803
137 Sang J, Wei P, Liu T, *et al.* A reconstructed $Cu_2P_2O_7$ catalyst for selective CO_2 electroreduction to multicarbon products. Angew Chem Int Ed, 2022, 61: e202114238
138 Long C, Liu X, Wan K, *et al.* Regulating reconstruction of oxide-derived Cu for electrochemical CO_2 reduction toward *n*-propanol. Sci Adv, 2023, 9: eadi6119
139 Wang S, Wang D, Tian B, *et al.* Synergistic Cu^+/Cu^0 on Cu_2O-Cu interfaces for efficient and selective C_{2+} production in electrocatalytic CO_2 conversion. Sci China Mater, 2023, 66: 1801–1809
140 Deng B, Huang M, Li K, *et al.* The crystal plane is not the key factor for CO_2-to-methane electrosynthesis on reconstructed Cu_2O microparticles. Angew Chem Int Ed, 2022, 61: e202114080
141 Mu S, Lu H, Wu Q, *et al.* Hydroxyl radicals dominate reoxidation of oxide-derived Cu in electrochemical CO_2 reduction. Nat Commun, 2022, 13: 3694
142 Gandionco KA, Kim J, Bekaert L, *et al.* Single-atom catalysts for the electrochemical reduction of carbon dioxide into hydrocarbons and oxygenates. Carbon Energy, 2024, 6: e410
143 Lum Y, Ager JW. Stability of residual oxides in oxide-derived copper catalysts for electrochemical CO_2 reduction investigated with ^{18}O labeling. Angew Chem Int Ed, 2018, 57: 551–554
144 Li CW, Ciston J, Kanan MW. Electroreduction of carbon monoxide to liquid fuel on oxide-derived nanocrystalline copper. Nature, 2014, 508: 504–507
145 Jiang K, Huang Y, Zeng G, *et al.* Effects of surface roughness on the electrochemical reduction of CO_2 over Cu. ACS Energy Lett, 2020, 5: 1206–1214
146 Mariano RG, McKelvey K, White HS, *et al.* Selective increase in CO_2 electroreduction activity at grain-boundary surface terminations. Science, 2017, 358: 1187–1192
147 Long C, Wan K, Chen Y, *et al.* Steering the reconstruction of oxide-derived Cu by secondary metal for electrosynthesis of *n*-propanol from CO. J Am Chem Soc, 2024, 146: 4632–4641
148 Martić N, Reller C, Macauley C, *et al.* $Ag_2Cu_2O_3$—A catalyst template material for selective electroreduction of CO to C_{2+} products. Energy Environ Sci, 2020, 13: 2993–3006
149 Rong Y, Liu T, Sang J, *et al.* Directing the selectivity of CO electrolysis to acetate by constructing metal-organic interfaces. Angew Chem Int Ed, 2023, 62: e202309893
150 Wang Q, Lei Y, Wang D, *et al.* Defect engineering in earth-abundant electrocatalysts for CO_2 and N_2 reduction. Energy Environ Sci, 2019, 12: 1730–1750
151 Shah SSA, Sufyan Javed M, Najam T, *et al.* Metal oxides for the electrocatalytic reduction of carbon dioxide: Mechanism of active sites, composites, interface and defect engineering strategies. Coord Chem Rev, 2022, 471: 214716
152 Cui B, Liu C, Zhang J, *et al.* Waste to wealth: Defect-rich Ni-incorporated spent $LiFePO_4$ for efficient oxygen evolution reaction. Sci China Mater, 2021, 64: 2710–2718
153 Yan X, Zhuang L, Zhu Z, *et al.* Defect engineering and characterization of active sites for efficient electrocatalysis. Nanoscale, 2021, 13: 3327–3345
154 Zhang Y, Tao L, Xie C, *et al.* Defect engineering on electrode materials for rechargeable batteries. Adv Mater, 2020, 32: 1905923
155 Zhu K, Shi F, Zhu X, *et al.* The roles of oxygen vacancies in electrocatalytic oxygen evolution reaction. Nano Energy, 2020, 73: 104761
156 Jiang W, Loh H, Low BQL, *et al.* Role of oxygen vacancy in metal oxides for photocatalytic CO_2 reduction. Appl Catal B-Environ, 2023, 321: 122079
157 Yang T, Lin L, Lv X, *et al.* Interfacial synergy between the Cu atomic layer and CeO_2 promotes CO electrocoupling to acetate. ACS Nano, 2023, 17: 8521–8529
158 Zhang J, Wang Y, Li Z, *et al.* Grain boundary-derived Cu^+/Cu^0 interfaces in CuO nanosheets for low overpotential carbon dioxide electroreduction to ethylene. Adv Sci, 2022, 9: 2200454
159 van Swygenhoven H, Farkas D, Caro A. Grain-boundary structures in polycrystalline metals at the nanoscale. Phys Rev B, 2000, 62: 831–838
160 Wang J, Cheng C, Huang B, *et al.* Grain-boundary-engineered La_2CuO_4 perovskite nanobamboos for efficient CO_2 reduction reaction. Nano Lett, 2021, 21: 980–987
161 Feng X, Jiang K, Fan S, *et al.* A direct grain-boundary-activity correlation for CO electroreduction on Cu nanoparticles. ACS Cent Sci, 2016, 2: 169–174
162 Thirathipviwat P, Sato S, Song G, *et al.* A role of atomic size misfit in lattice distortion and solid solution strengthening of TiNbHfTaZr high entropy alloy system. Scripta Mater, 2022, 210: 114470
163 Dholabhai PP, Uberuaga BP. Beyond coherent oxide heterostructures: Atomic-scale structure of misfit dislocations. Advcd Theor Sims, 2019, 2: 1900078
164 Li Z, Fu JY, Feng Y, *et al.* A silver catalyst activated by stacking faults for the hydrogen evolution reaction. Nat Catal, 2019, 2: 1107–1114
165 Lv J, Yin R, Zhou L, *et al.* Microenvironment engineering for the electrocatalytic CO_2 reduction reaction. Angew Chem Int Ed, 2022, 61: e202207252
166 Chen J, Wang L. Effects of the catalyst dynamic changes and influence of the reaction environment on the performance of electrochemical CO_2 reduction. Adv Mater, 2022, 34: 2103900
167 Jiang H, Luo R, Li Y, *et al.* Recent advances in solid-liquid-gas three-phase interfaces in electrocatalysis for energy conversion and storage. EcoMat, 2022, 4: e12199
168 Fei H, Dong J, Chen D, *et al.* Single atom electrocatalysts supported on graphene or graphene-like carbons. Chem Soc Rev, 2019, 48: 5207–5241
169 van Deelen TW, Hernández Mejía C, de Jong KP. Control of metal-support interactions in heterogeneous catalysts to enhance activity and selectivity. Nat Catal, 2019, 2: 955–970
170 Yue P, Fu Q, Li J, *et al.* Triple-phase electrocatalysis for the enhanced CO_2 reduction to HCOOH on a hydrophobic surface. Chem Eng J, 2021, 405: 126975
171 Zhou L, Li C, Lv J, *et al.* Synergistic regulation of hydrophobicity and basicity for copper hydroxide-derived copper to promote the CO_2 electroreduction reaction. Carbon Energy, 2023, 5: e328
172 Park S, Grigioni I, Alkayyali T, *et al.* High carbon efficiency in CO-to-alcohol electroreduction using a CO reservoir. Joule, 2023, 7: 2335–2348
173 Duan GY, Li XL, Ding GR, *et al.* Highly efficient electrocatalytic CO_2 reduction to C_{2+} products on a poly(ionic liquid)-based Cu^0-Cu^I tandem catalyst. Angew Chem Int Ed, 2022, 61: e202110657
174 Duan GY, Li XQ, Chen JW, *et al.* Poly(ionic liquid) boosts overall performance of electrocatalytic reduction of low concentration of CO gas. Chem Eng J, 2023, 451: 138491
175 Rabiee H, Ge L, Zhang X, *et al.* Gas diffusion electrodes (GDEs) for electrochemical reduction of carbon dioxide, carbon monoxide, and dinitrogen to value-added products: A review. Energy Environ Sci, 2021, 14: 1959–2008
176 Nguyen TN, Dinh CT. Gas diffusion electrode design for electrochemical carbon dioxide reduction. Chem Soc Rev, 2020, 49: 7488–7504
177 Wakerley D, Lamaison S, Wicks J, *et al.* Gas diffusion electrodes, reactor designs and key metrics of low-temperature CO_2 electrolysers. Nat Energy, 2022, 7: 130–143
178 Xu Q, Xu A, Garg S, *et al.* Enriching surface-accessible CO_2 in the zero-gap anion-exchange-membrane-based CO_2 electrolyzer. Angew Chem Int Ed, 2023, 62: e202214383
179 Weng LC, Bell AT, Weber AZ. Towards membrane-electrode assembly systems for CO_2 reduction: A modeling study. Energy Environ Sci, 2019, 12: 1950–1968
180 Hasa B, Cherniack L, Xia R, *et al.* Benchmarking anion-exchange membranes for electrocatalytic carbon monoxide reduction. Chem Catal, 2023, 3: 100450
181 Rabinowitz JA, Ripatti DS, Mariano RG, *et al.* Improving the energy efficiency of CO electrolysis by controlling Cu domain size in gas

 © Science China Press 2024

diffusion electrodes. ACS Energy Lett, 2022, 7: 4098–4105
182 Ripatti DS, Veltman TR, Kanan MW. Carbon monoxide gas diffusion electrolysis that produces concentrated C_2 products with high single-pass conversion. Joule, 2019, 3: 240–256
183 Higgins D, Hahn C, Xiang C, *et al.* Gas-diffusion electrodes for carbon dioxide reduction: A new paradigm. ACS Energy Lett, 2018, 4: 317–324
184 Lees EW, Mowbray BAW, Parlane FGL, *et al.* Gas diffusion electrodes and membranes for CO_2 reduction electrolysers. Nat Rev Mater, 2022, 7: 55–64
185 Xu Q, Garg S, Moss AB, *et al.* Identifying and alleviating the durability challenges in membrane-electrode-assembly devices for high-rate CO electrolysis. Nat Catal, 2023, 6: 1042–1051
186 Wang Q, Dong H, Yu H, *et al.* Enhanced performance of gas diffusion electrode for electrochemical reduction of carbon dioxide to formate by adding polytetrafluoroethylene into catalyst layer. J Power Sources, 2015, 279: 1–5
187 Rabiee H, Heffernan JK, Ge L, *et al.* Tuning flow-through Cu-based hollow fiber gas-diffusion electrode for high-efficiency carbon monoxide (CO) electroreduction to C2+ products. Appl Catal B-Environ, 2023, 330: 122589
188 Ji Y, Shi Y, Liu C, *et al.* Plasma-regulated N-doped carbon nanotube arrays for efficient electrosynthesis of syngas with a wide CO/H_2 ratio. Sci China Mater, 2020, 63: 2351–2357
189 Qiu N, Li J, Wang H, *et al.* Emerging dual-atomic-site catalysts for electrocatalytic CO_2 reduction. Sci China Mater, 2022, 65: 3302–3323
190 Wang Z, Zou G, Park JH, *et al.* Progress in design and preparation of multi-atom catalysts for photocatalytic CO_2 reduction. Sci China Mater, 2024, 67: 397–423
191 Yang C, Gao Z, Wang D, *et al.* Bimetallic phthalocyanine heterostructure used for highly selective electrocatalytic CO_2 reduction. Sci China Mater, 2022, 65: 155–162
192 Yang M, Sun J, Qin Y, *et al.* Hollow CoFe-layered double hydroxide polyhedrons for highly efficient CO_2 electrolysis. Sci China Mater, 2022, 65: 536–542
193 Gong L, Zhang D, Lin CY, *et al.* Catalytic mechanisms and design principles for single-atom catalysts in highly efficient CO_2 conversion. Adv Energy Mater, 2019, 9: 1902625
194 Yang Z, Gao W, Jiang Q. A machine learning scheme for the catalytic activity of alloys with intrinsic descriptors. J Mater Chem A, 2020, 8: 17507–17515
195 Vasilyev DV, Shyshkanov S, Shirzadi E, *et al.* Principal descriptors of ionic liquid co-catalysts for the electrochemical reduction of CO_2. ACS Appl Energy Mater, 2020, 3: 4690–4698
196 Yuan H, Li Z, Zeng XC, *et al.* Descriptor-based design principle for two-dimensional single-atom catalysts: Carbon dioxide electroreduction. J Phys Chem Lett, 2020, 11: 3481–3487
197 Gao W, Xu Y, Xiong H, *et al.* CO binding energy is an incomplete descriptor of Cu-based catalysts for the electrochemical CO_2 reduction reaction. Angew Chem, 2023, 135: e202313798
198 Yin Z, Yu J, Xie Z, *et al.* Hybrid catalyst coupling single-atom Ni and nanoscale Cu for efficient CO_2 electroreduction to ethylene. J Am Chem Soc, 2022, 144: 20931–20938
199 Feng J, Zhang L, Liu S, *et al.* Modulating adsorbed hydrogen drives electrochemical CO_2-to-C_2 products. Nat Commun, 2023, 14: 4615
200 Zhang L, Yang X, Yuan Q, *et al.* Elucidating the structure-stability relationship of Cu single-atom catalysts using *operando* surface-enhanced infrared absorption spectroscopy. Nat Commun, 2023, 14: 8311
201 Jordaan SM, Wang C. Electrocatalytic conversion of carbon dioxide for the Paris goals. Nat Catal, 2021, 4: 915–920
202 Chang F, Xiao M, Miao R, *et al.* Copper-based catalysts for electrochemical carbon dioxide reduction to multicarbon products. Electrochem Energy Rev, 2022, 5: 4
203 Wang X, Hu Q, Li G, *et al.* Recent advances and perspectives of electrochemical CO_2 reduction toward C_{2+} products on Cu-based catalysts. Electrochem Energy Rev, 2022, 5: 28
204 Dai Y, Kong F, Tai X, *et al.* Advances in graphene-supported single-atom catalysts for clean energy conversion. Electrochem Energy Rev, 2022, 5: 22
205 Kou Z, Li X, Wang T, *et al.* Fundamentals, on-going advances and challenges of electrochemical carbon dioxide reduction. Electrochem Energy Rev, 2022, 5: 82–111
206 Li L, Liu Z, Yu X, *et al.* Achieving high single-pass carbon conversion efficiencies in durable CO_2 electroreduction in strong acids *via* electrode structure engineering. Angew Chem Int Ed, 2023, 62: e202300226
207 Ma Z, Yang Z, Lai W, *et al.* CO_2 electroreduction to multicarbon products in strongly acidic electrolyte *via* synergistically modulating the local microenvironment. Nat Commun, 2022, 13: 7596
208 Gu J, Liu S, Ni W, *et al.* Modulating electric field distribution by alkali cations for CO_2 electroreduction in strongly acidic medium. Nat Catal, 2022, 5: 268–276
209 Kurihara R, Nagita K, Ohashi K, *et al.* Carbon monoxide reduction reaction to produce multicarbon products in acidic electrolytes using gas diffusion electrode loaded with copper nanoparticles. Adv Mater Inter, 2024, 11: 2300731

Acknowledgements Zhao W would like to acknowledge the support from the Natural Science Foundation of Jiangsu Province (BK20210189), the National Natural Science Foundation of China (22176086), the State Key Laboratory of Pollution Control and Resource Reuse, the Fundamental Research Funds for the Central Universities (021114380183, 021114380189, and 021114380199), the Research Funds from Frontiers Science Center for Critical Earth Material Cycling of Nanjing University, the Research Funds for Jiangsu Distinguished Professor, and the Carbon Peaking and Carbon Neutrality Technological Innovation Foundation of Jiangsu Province (BE2022861). Sun X Would like to thank the support from the National Natural Science Foundation of China (82272138 and 81971738) and Jiangsu Province Outstanding Youth Fund (BK20220086). Lin R would like to thank the support from the National Natural Science Foundation of China (52276177).

Author contributions Zhu W supervised the project and organized the collaboration. Zhao W wrote the manuscript and Liu J, Wang G, Wang X, Yang C, Li J, Wang Y, Sun X, Lin R and Zuo G revised the manuscript. All authors discussed, edited and commented on the manuscript.

Conflict of interest The authors declare that they have no conflict of interest.

Wen Zhao is pursuing a Master degree at the School of the Environment, Nanjing University, under the supervision of Prof. Wenlei Zhu. Her research focuses on the electrochemical reduction of carbon monoxide.

Wenlei Zhu is a professor at the School of the Environment, Nanjing University. He obtained his BSc and PhD degrees from Nanjing University and Brown University, respectively, followed by postdoc at Washington University in St. Louis, Columbia University in the City of New York and University of Delaware for several years. His current research interests focus on resource utilization of greenhouse gases.

© Science China Press 2024

铜基催化剂用于一氧化碳电还原为多碳产品

赵雯[1], 刘娟[1], 王光滔[1], 王新天[1], 杨传举[1], 李剑[2], 王锆葶[1], 孙晓莲[3], 林日琛[4], 左淦丞[1,5], 朱文磊[1*]

摘要 电化学二氧化碳还原(ECO_2R)是一种将碳和可再生能源的能量储存在多碳产品(C_{2+})的化学键中的有效途径. 然而, 反应涉及的复杂步骤为CO_2直接转化为C_{2+}设置了巨大的障碍. 一种利用CO作为"中转站", 通过串联ECO_2R和电化学CO还原(ECOR)以提高生产C_{2+}的选择性和反应速率的策略引起了人们的广泛关注. 本文总结了铜基电催化剂在ECOR中催化特定C_{2+}生成的设计策略. 其次, 从各个方面总结了催化剂工程的代表性设计策略, 并介绍了电解反应器改进方面的最新进展. 最后, 阐述了该研究领域面临的主要挑战和未来前景. 这些见解和观点将为铜基电催化剂的设计提供有益指导.

© Science China Press 2024